Dwell-fatigue crack growth behaviour of Alloy 709

Yan, Jin; Yu, Suyang; Ding, Rengen; Li, Hangyue; Rabiei, Afsaneh; Bowen, Paul

DOI:
10.1016/j.actamat.2023.118808

Document Version
Publisher's PDF, also known as Version of record

Citation for published version (Harvard):
Yan, J, Yu, S, Ding, R, Li, H, Rabiei, A & Bowen, P 2023, 'Dwell-fatigue crack growth behaviour of Alloy 709', *Acta Materialia*, vol. 249, 118808. https://doi.org/10.1016/j.actamat.2023.118808

Acta Materialia 249 (2023) 118808

Contents lists available at ScienceDirect

Acta Materialia

journal homepage: www.elsevier.com/locate/actamat

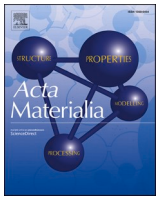

Full length article

Dwell-fatigue crack growth behaviour of Alloy 709

Jin Yan [a], Suyang Yu [a], Rengen Ding [a], Hangyue Li [a,*], Afsaneh Rabiei [b], Paul Bowen [a]

[a] School of Metallurgy and Materials, University of Birmingham, Edgbaston, Birmingham B15 2TT, United Kingdom
[b] Advanced Materials Research Laboratory (AMRL), Department of Mechanical and Aerospace Engineering, North Carolina State University, Raleigh NC 27695, United States

ARTICLE INFO

Keywords:
Dwell-fatigue crack growth
Creep-fatigue interactions
Crack growth mechanisms
Alloy 709
Type 316H
Austenitic stainless steels

ABSTRACT

Dwell-fatigue crack growth behaviour of an advanced austenitic stainless steel Alloy 709 has been investigated and compared with that of a conventional Type 316H stainless steel. The test procedure employed alternation of 1 h dwell-fatigue loading and 0.25 Hz fast cycling so that crack growth rates (da/dN) obtained from dwell-fatigue loading can be compared to those purely result from fatigue mechanism on the same test-piece. Tests were conducted at 550, 650 and 750 °C in air using 0.5 T compact tension test-pieces under a fixed maximum load of 8 kN and a stress ratio, R, of 0.1. For the investigated temperature and ΔK ranges, crack growth mechanisms of fatigue alone, creep alone and mixed fatigue-creep have all been observed. Detailed fractographic and metallographic observations were conducted to interpret failure mechanisms and regimes of different failure modes. Compared to crack growth rates obtained under 0.25 Hz fatigue loading, dwell-fatigue produces: no obvious increases in crack growth rates at a test temperature of 550 °C; a moderate increase (~ 2–5 times) at a test temperature of 650 °C; and, over a tenfold increase at a test temperature of 750 °C. Compared to 316H, Alloy 709 has much improved resistance against creep-fatigue crack growth, here confirmed at the single test temperature of 650 °C.

1. Introduction

Creep-resistant austenitic stainless steels are an important class of high temperature materials for structural applications in nuclear power plants. To meet the continuous drive towards higher thermal efficiency, better economics, and greater safety margin and design capability for new generation power plants, advanced alloys with complex chemical compositions have been developed in recent years. Alloy 709 belongs to this class of alloys and is currently under consideration for structural applications in sodium-cooled fast reactors. Safe operation of nuclear power plants requires a comprehensive understanding of material performance under prolonged stressing in complex operating cycles and environments. One essential element is the capability to predict remaining life and safe inspection intervals of components containing flaws, which relies on the understanding of crack growth resistance under fatigue loading alone, creep loading alone, and under combined loading. Indeed, crack growth data are required in many high temperature Code cases for assessing structure integrity, e.g. ASME, R5, RCC-MR [1]. As a relatively new alloy such databases and detailed mechanistic understanding have not been established to date. The current paper is one of a series of papers to characterise crack growth behaviour in Alloy 709. It focuses on combined influence of cycle-dependant fatigue crack growth and time-dependant creep crack growth.

Creep-fatigue crack growth in metals is often characterised by adaptation of a dwell-fatigue loading waveform which contains a static hold within a normal fatigue loading waveform – typically tensile dwell at maximum load. It is generally observed that the crack growth is cycle-dependant at short dwell times and/or high frequency, but it often becomes time-dependant with increasing dwell times and/or reduced cycle frequency [2]. Such transitions occur when a critical hold time is exceeded, and such hold time varies with alloy composition and microstructure, temperature, and stress levels. Under certain conditions, fatigue and creep mechanisms both operate, resulting in “fatigue-creep interactions” [2].

When considering crack growth rates under the conjoint effects of fatigue and creep, it is important to identify and to distinguish the nature of intergranular damage resulting from dwell time. There are two main types of intergranular damage, referred as “creep-ductile” and “creep-brittle” in the literature [3]. Different crack growth parameters may then need to be employed to characterise crack growth. The creep-brittle

* Corresponding author.
E-mail address: h.y.li.1@bham.ac.uk (H. Li).

https://doi.org/10.1016/j.actamat.2023.118808
Received 12 October 2022; Received in revised form 23 January 2023; Accepted 21 February 2023
Available online 25 February 2023

Table 1
Chemical composition of Alloy 709 and Type 316H (wt%).

	Cr	Ni	Mo	N	Ti	Nb
Alloy 709	19.69	25.00	1.46	0.14	<0.001	0.23
316H	16.61	10.26	2.006	0.0315	0.005	0.005
	C	Mn	Si	P	S	B
Alloy 709	0.063	0.88	0.28	<0.005	<0.001	0.0022
316H	0.041	1.536	0.329	0.036	0.001	–

phenomenon often occurs in alloys which possess very high monotonic strength and creep strength, such as in some nickel-based superalloys [4]. As a relatively small amount of creep deformation is present ahead of the moving crack tip in creep-brittle scenario, fatigue crack growth rates can often be rationalised by linear elastic fracture mechanics parameters, such as the stress intensity factor range ΔK. The failure mechanisms involved are often related to the presence of embrittlement species such as oxygen. It should be noted that such accelerated crack growth due to environmental embrittlement will disappear when tests are conducted in vacuum and in which oxygenated environment is removed [4]. Creep crack growth in austenitic stainless steels is generally considered to be "creep-ductile" in nature, as crack growth is accompanied by significant amounts of time-dependant plastic deformation [5].

Representative experimental work is given, for example, by Sadananda and Shahinian [6].They studied crack growth behaviour in Types 316 and Type 304 austenitic stainless steels at 593 °C under cyclic, dwell- (60 s)-cyclic, and static loading both in air and in vacuum. Faster crack growth rates were measured under dwell-cyclic loading (~10 times increase) at a given ΔK value. This effect is insensitive to environment as similar results are seen in vacuum. The fracture mechanism was observed to change to intergranular under both dwell-cyclic loading and static loading, implying time-dependant creep damage. In addition, the authors concluded that a simple summation of crack growth under cyclic (fatigue) and crack growth under static (creep) could predict crack growth rates under combined dwell-fatigue loading. In addition to

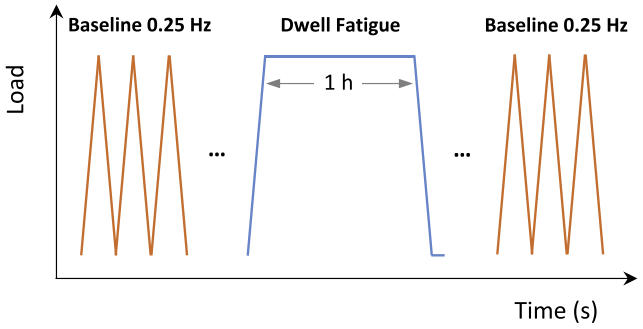

Fig. 1. Schematic drawing of the loading sequence adopted.

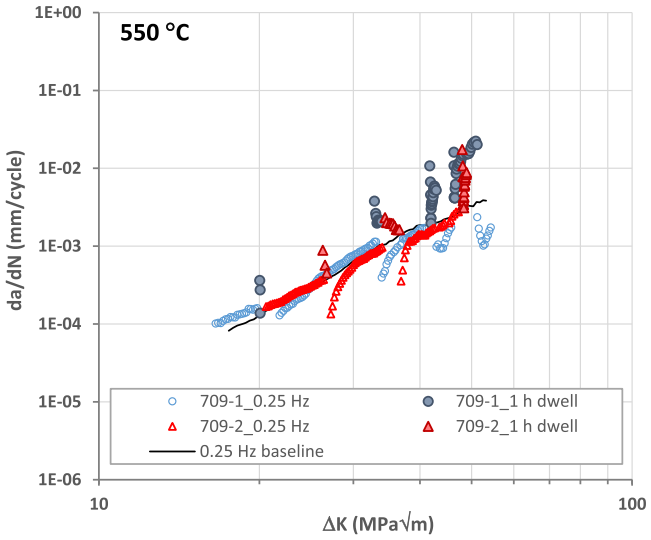

Fig. 2. Crack growth resistance curves obtained in Alloy 709 at 550 °C in air using alternation of dwell fatigue (1 h holding at the maximum load) and fatigue (0.25 Hz) loading, $R = 0.1$.

Table 2
Overview of all tests, listing the range of ΔK and maximum ligament stresses at the crack tip* corresponding to each dwell-fatigue loading block within the individual tests. The associated total number of cycles and fracture surface morphology were also provided.

Temperature and Environment	Test-piece ID	Demensions W, B, B_n (mm)	1 h dwell- fatigue loading block	ΔK range (MPa√m)	σ_{max} range* (MPa)	Number of cycles applied	Fracture surface morphology**
550 °C Air	709–1	26.12	1st	20.0 – 20.1	239–244	90	TG
		13.03	2nd	32.9 – 33.9	478–499	118	TG+IG
		12.06	3rd	41.7 – 42.9	670–697	47	TG+IG
			4th	46.1 – 51.4	796–889	55	TG+IG
550 °C Air	709–2	25.93	1st	26.2 – 26.8	341–346	313	TG
		12.01	2nd	34.3 – 36.8	502–545	328	TG+IG
		11.05	3rd	48.0 – 49.0	801–813	22	TG+IG
650 °C Air	709–3	25.91	1st	17.8 – 18.3	215–222	354	TG
		12.99	2nd	31.8 – 39.7	465–639	753	IG
		11.16	3rd	45.0 – 66.7	763–1205	93	MVC
650 °C Air	709–4	26.00	1st	26.9 – 27.6	368–379	54	TG
		13.06	2nd	34.4 – 38.3	511–593	72	IG
		11.90	3rd	51.8 – 60.0	871–1108	3	MVC
650 °C Vacuum	709–5	26.12	1st	30.5 – 31.9	433–458	85	IG
		12.94	2nd	43.5 – 58.0	672–1024	26	IG+MVC
		12.01					
750 °C Air	709–6	25.81	1st	20.5 – 22.2	242–268	189	IG+MVC
		11.94	2nd	25.7 – 29.7	326–400	75	MVC
		11.00	3rd	31.9 – 52.7	442–899	33	MVC
650 °C Air	316H	26.64	1st	21.2 – 26.2	249–330	448	IG
		11.81	2nd	32.5 – 42.9	447–665	53	IG+MVC
		10.89	3rd	49.8 – 52.4	820–879	0.5	MVC

* Ligament stress at the crack tip is estimated by a summation of tensile [$\sigma_T = \frac{P}{B_n(W-a)}$] and bending [$\sigma_B = \frac{6P\left(a+\frac{W-a}{2}\right)}{B_n(W-a)^2}$] stresses without considering stress concentration and creep deformation.

** TG: Transgranular with fatigue striations; IG: intergranular cavitation; and MVC: microvoid coalescence.

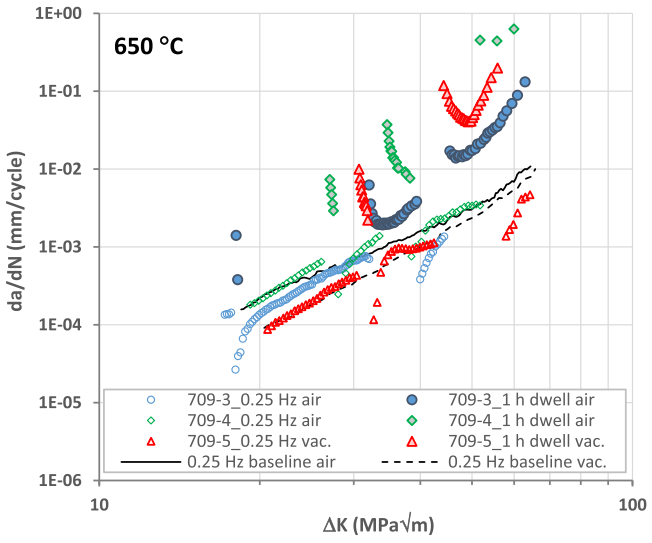

Fig. 3. Crack growth resistance curves obtained in Alloy 709 at 650 °C in air and vacuum using alternate sequences of dwell fatigue (1 h hold at maximum load) and fatigue (0.25 Hz) loading, $R = 0.1$.

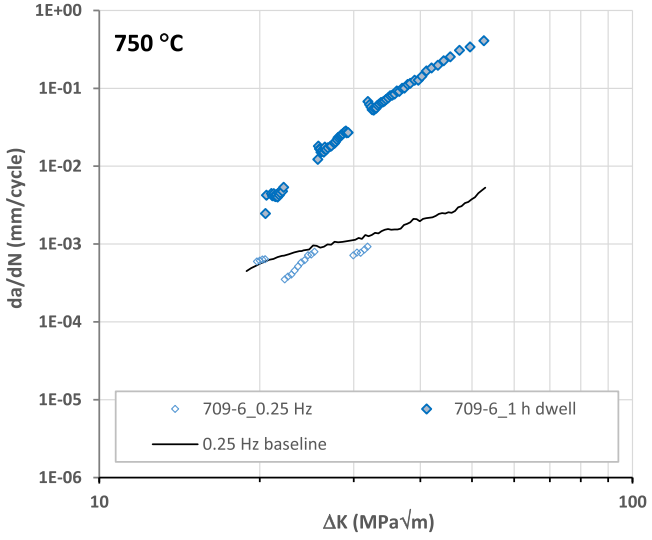

Fig. 4. Crack growth resistance curves obtained in Alloy 709 at 750 °C in air using alternate sequences of dwell fatigue (1 h hold at the maximum load) and fatigue (0.25 Hz) loading, $R = 0.1$.

studies on crack growth behaviour [6–8], there are also numerous studies addressing total fatigue life of smooth cylindrical test-pieces in austenitic stainless steels under creep-fatigue interactions (e.g. AISI 304 [9,10], 316 [11–13], Type 316 L [13–15], Type 316LN [13]). It is generally observed that creep-fatigue loading is more detrimental than creep or fatigue loading alone. Recently some crack growth data of Alloy 709 under dwell-fatigue loading have been published by Shaber et al. [16]. They employed dwell times of 60 and 600 s, and at test temperatures of 600 and 700 °C. Their results indicate little time-dependant contribution to total crack growth under a hold-time of 60 s, while under 600 s dwell a small increase, ~2 times, was indeed observed. Based on growth data and measurements of load-line displacement, they concluded that crack growth in Alloy 709 is creep-brittle in nature. The superior resistance against creep-fatigue crack growth in Alloy 709 may be true due to its superior creep strength [16]. However, the argument of "creep-brittle" behaviour in Alloy 709 is open to question. Real-time SEM observations of interactions between fatigue and creep mechanisms in Alloy 709 at a temperature of 750 °C were reported recently by Lall et al. [5]. They employed a series of dwell times, i.e. 1-s, 1-min and

Table 3

A and m values of the Paris Law $\frac{da}{dN} = A(\Delta K)^m$, for fatigue, and dwell-fatigue crack growth resistance curves of Alloy 709 obtained at temperatures of 550, 650 and 750 °C in air.

Temperature	Test type	A [mm/cycle]	m	ΔK range (MPa√m)
550 °C	Fatigue	1.27×10^{-08}	3.1	20–45
650 °C	Fatigue	1.04×10^{-07}	2.6	20–45
750 °C	Fatigue	3.57×10^{-06}	1.7	20–45
550 °C	Dwell-Fatigue	1.06×10^{-14}	7.2	37–52
650 °C	Dwell-Fatigue	3.44×10^{-13}	6.3	35–55
750 °C	Dwell-Fatigue	1.63×10^{-10}	5.6	20–50

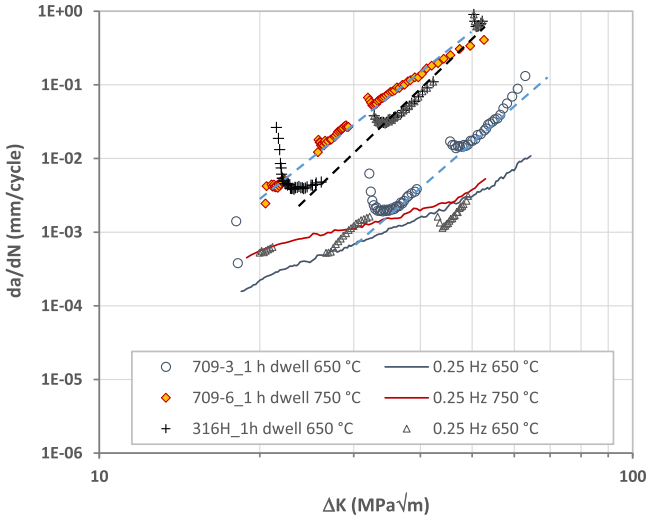

Fig. 5. Comparisons of crack growth resistance curves of Alloy 709 obtained at different temperatures, and 316H obtained at 650 °C. Note that the dashed lines are the trendlines of steady state crack growth under 1 h dwell loading.

1-h. They demonstrated that with 1-s dwell time predominantly transgranular striated crack growth is found. With dwell time increased to 1-min, grain boundary voids can form during the 1-min period, leading to predominantly intergranular crack path. Intermittent crack growth was observed, i.e., microvoids form on grain boundary during dwell period, and they link during cycling loading to advance the crack. Under 1-h dwell-fatigue condition, in addition to a fully intergranular crack growth mechanism, significant crack blunting occurs compared to 1-min dwell-fatigue loading.

The current work focuses on crack growth behaviour under dwell-fatigue loading at long dwell time. The experimental procedure adopts block sequences of a 1 h dwell-fatigue and fatigue loading (0.25 Hz). Test temperatures considered are from 550 °C (close to the envisaged application temperature) to 750 °C. In addition, tests have also been conducted under the same test procedures for Type 316H austenitic stainless steel at 650 °C to gain a better understanding of the potential of the austenite stainless steel Alloy 709.

2. Experimental

2.1. Materials

Alloy 709 material used in the current study was supplied by Oak Ridge National Laboratory, US and produced by Carpenter Technology Corporation in plate form. After forging and rolling, the material was annealed at 1100 °C, followed by water quenching. Type 316H (UNS S31609) stainless steel used in this study was acquired from SIJ Acroni Steel. The 316H alloy was solution annealed at a minimum temperature of 1052 °C and then water quenched. Nominal chemical compositions of both Alloy 709 and 316H are given in Table 1.

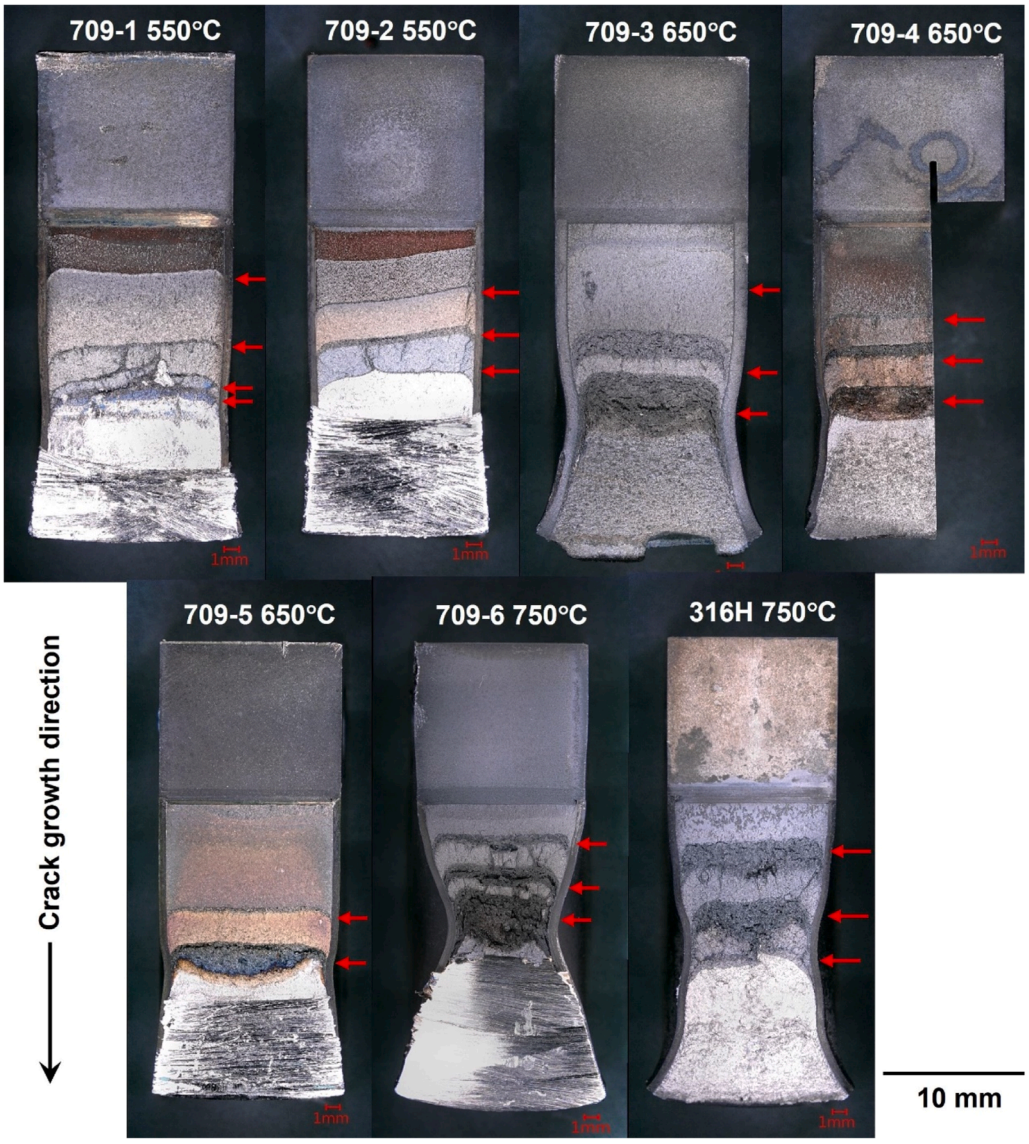

Fig. 6. Optical macrographs of fracture surfaces. Note that the dwell-fatigue regions are indicated by an arrow.

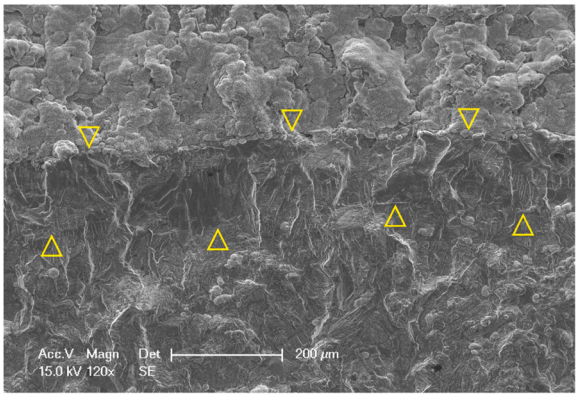

(a)

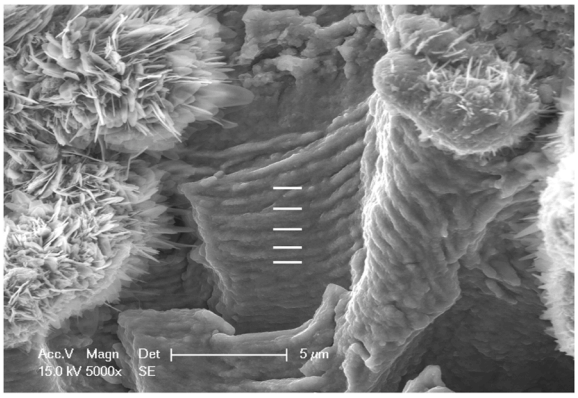

(b)

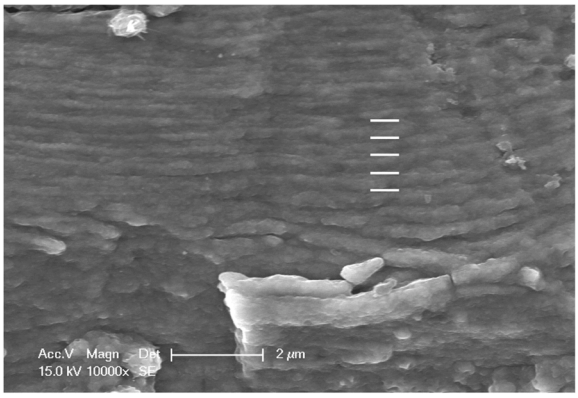

(c)

Fig. 7. SEM fractographs taken from the first dwell fatigue crack growth region of the test-piece 709–1 ($\Delta K \sim 20$ MPa$\sqrt{m}$) after testing at 550 °C: (a) overview of the region showing a predominant transgranular morphology; and a comparison of striations formed at the beginning of the region, (b); and at the end of the region, (c). Note that fatigue crack growth direction is from the top to bottom in all cases, also the beginning and end of dwell fatigue crack growth region are arrowed in (a).

2.2. Crack growth resistance tests

Six dwell-fatigue crack growth tests were conducted at 550, 650 and 750 °C in air, and one test was conducted in vacuum at the temperature of 650 °C. A compact tension (CT) test-piece geometry was adopted. The width (W) of all test-pieces is 26 mm. Due to a variation of original plate thickness, the thickness of the test-pieces (B) is either 13 or 12 mm. Side-grooves were machined on both side surfaces. The depth of each side-groove is 0.5 mm, apart from in test-piece 709–3, where the depth of each side groove is 1 mm. The resultant net-section thickness is thus either 11 or 12 mm – see Table 2 for details. All test-pieces were extracted in an orientation that the crack plane is normal to the rolling direction and the crack growth direction is parallel to transverse direction, i.e. L-T.

Test-pieces were fatigue precracked at room temperature using an Amsler Vibrophore operating at a frequency of ~80 Hz. After pre-cracking, samples were transferred to a screw-driven servo-electric mechanical testing machine for high temperature crack growth testing. A direct current potential drop (d.c.p.d.) technique was used to monitor and record crack growth in all cases.

Dwell-fatigue crack growth tests utilised a trapezoidal loading waveform comprising a one second ramp from minimum to maximum load, one hour holding at maximum load, one second ramp to minimum load, and one second holding at minimum load, i.e. 1–3600–1–1. The load ratio (R = minimum load/maximum load) used was 0.1. A sinusoidal fatigue loading waveform of a frequency of 0.25 Hz (with the same maximum load and R ratio) was introduced to interrupt 1 h dwell-fatigue cycles in block sequences. The introduction of 0.25 Hz fast cycling was made based on following two criteria: (1) the required amount of crack growth is achieved, ~1–4 mm in this study; (2) crack has stopped growing for three days. A minimum growth length of 1 mm is required before returning to dwell-fatigue block loading. Sequences of 2–4 blocks of 1 h dwell-fatigue loads were applied for each test. A schematic demonstration of the procedure is given in Fig. 1. Such a testing procedure can reduce testing time significantly. It can also generate a baseline of fatigue crack growth rates so that comparisons between different loading waveforms can be made readily for an individual test-piece. In order to isolate the influence of unloading and reloading in the dwell-fatigue loading waveform on crack growth behaviour, an additional test was conducted at each temperature by replacing 1–3600–1–1 loading blocks with sustained loading blocks. It is only in these tests utilising static loading blocks that the load-line crack opening displacement (COD) was measured and from which the percentage of time-dependant displacement rate to total displacement rate was calculated.

In general, the maximum applied load was kept constant throughout for all tests at 8 kN. Crack growth resistance was evaluated over a ΔK range of 20 to 50 MPa$\sqrt{m}$ with associated crack lengths ranging from $0.2 < a/W < 0.7$ (where a is the crack depth and W is the width of the test-piece). Attempts were made to interrupt tests before catastrophic failure, the furnace was switched off and the test-pieces were then put under fatigue loading at room temperature in order to break open the test-pieces into two halves. Note that four test-pieces were finally cut open using a handsaw after some initial post-interruption room temperature fatigue crack growth.

The linear elastic stress intensity factor range, ΔK for a CT test-piece geometry is calculated using Eq. (1) [17]:

$$\Delta K = \frac{\Delta P}{\sqrt{BB_n}\sqrt{W}} \frac{2 + a/W}{(1 - a/W)^{1.5}} \left(0.886 + 4.64(a/W) - 13.32(a/W)^2 + 14.72(a/W)^3 - 5.6(a/W)^4\right). \quad (1)$$

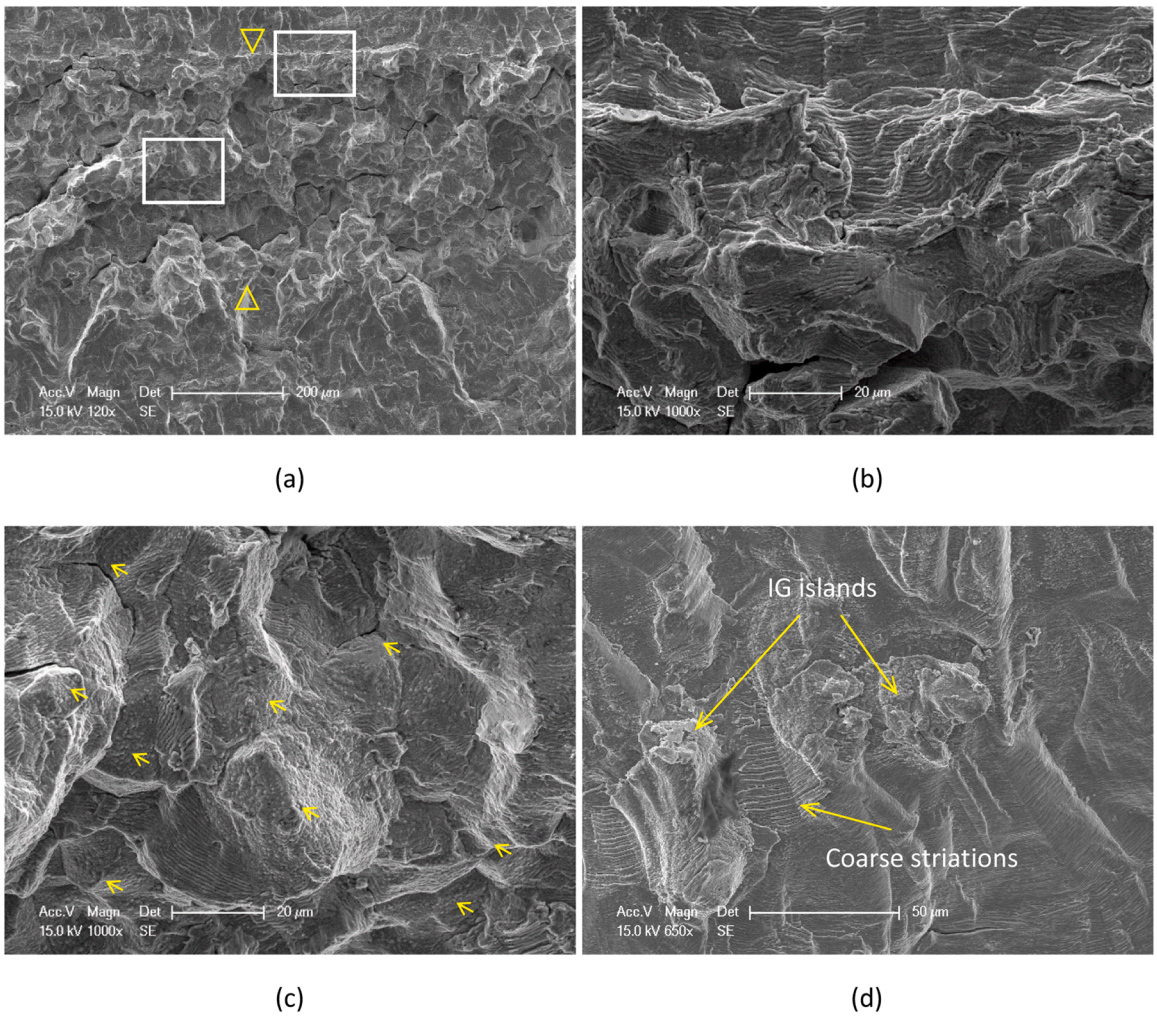

Fig. 8. SEM fractographs taken from the second dwell fatigue crack growth region of the test-piece 709–2 ($\Delta K \sim 34 - 37$ MPa$\sqrt{m}$) after testing at 550 °C: (a) overview of the region showing an intergranular-like morphology; (b) beginning of the region; (c) in the middle of the region, arrows indicate intergranular islands; and (d) ahead at region. Note that fatigue crack growth direction is from the top to bottom in all cases, also the beginning and end of dwell fatigue crack growth region are arrowed in (a).

where a is the crack depth, W is the width of the test-piece, ΔP is the load range, B is the thickness of the test-piece and B_n is the net section thickness after subtracting the depth of the side-grooves.

2.3. Characterization of failure mechanisms

After testing, fracture surfaces were examined using both optical microscopy (OM) and scanning electron microscopy (SEM) to observe the crack growth mechanisms. To further verify these crack growth mechanisms, one half of the fractured test-piece was sectioned perpendicular to the fracture surface and parallel to the crack growth direction for observation of underlying damage using OM, SEM and electron backscattered diffraction (EBSD) mapping. Transmission electron microscopy (TEM) investigation was also performed for selected tests where cross-sectional samples were extracted from the fracture surfaces using an FEI Quanta 3D dual beam focussed ion beam (FIB) microscope. A Pt coating was used to protect the fracture surface from being milled away. To minimize the amorphous layer and any damage caused by FIB milling, final cleaning was conducted at 5 kV.

3. Results

3.1. Dwell-fatigue crack growth resistance curves

Crack growth resistance curves for Alloy 709 are plotted in terms of da/dN versus ΔK in Figs. 2–4 for temperatures 550, 650 and 750 °C respectively. Corresponding to alternating loading waveform between 1 h dwell-fatigue and 0.25 Hz fast fatigue, the crack growth resistance curves presented comprise a series of segments resulting from the two waveforms. The applied load range was fixed for all tests with a maximum load of 8 kN and a load ratio of 0.1. Under such loading conditions, it is understood that both stress intensity factor range (ΔK) and net section stresses increase with an increase of crack length. Table 2 lists the range of ΔK, the range of nominal stress at crack tip, the total number of 1 h dwell-fatigue cycles and the observed crack growth mechanisms for every 1 h dwell-fatigue loading blocks within each test. In order to understand the transient crack grow behaviour due to waveform changes, a crack growth resistance curve obtained from continuous fast fatigue loading (0.25 Hz) is provided for comparison, this curve is referred as “0.25 Hz baseline” in the figures.

Unlike crack growth resistance curves obtained under continuous 0.25 Hz cycling (which shows a linear relationship between log(da/dN) and log(ΔK) (with values of Paris constants, A and m, given in Table 3), crack growth resistance curves obtained under 1 h dwell-fatigue loading

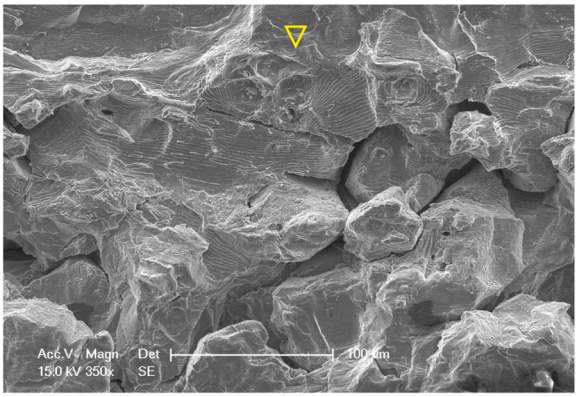

(a)

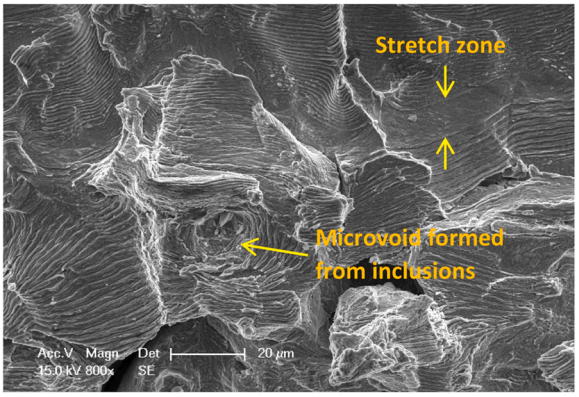

(b)

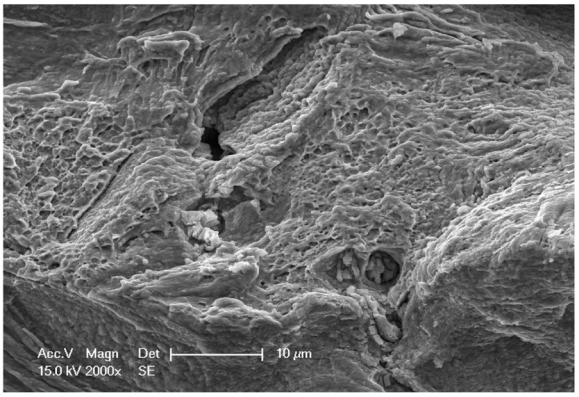

(c)

Fig. 9. SEM fractographs taken from the third dwell fatigue crack growth region of the test-piece 709–1 ($\Delta K \sim 42$ MPa$\sqrt{m}$) after testing at 550 °C: (a) an overview of the region showing both intergranular cracking and transgranular striations; (b) beginning of the region, showing nearly continuous striations following a continuous stretch zone (arrowed); (c) close-up of grain boundary morphology showing formation of microvoids. Note that fatigue crack growth direction is from the top to bottom in all cases, also the beginning of the dwell fatigue crack growth region is arrowed in (a).

exhibit unusual trends which vary with test temperature. At a test temperature of 550 °C (Fig. 2), dwell-fatigue crack growth rates initially accelerate after transfer from 0.25 Hz cycling, but these rates then exhibit a sharp retardation with further crack extension. There are signs of continuous crack growth when ΔK values exceed 32 MPa$\sqrt{m}$ (for example in the second dwell-fatigue sequence for test-piece 709–2), but stable (accelerating) crack growth rates with crack extension were never established under ΔK values of less than 40 MPa$\sqrt{m}$. In the third dwell-fatigue segment ($\Delta K > 41.7$ MPa$\sqrt{m}$), crack growth rate increases sharply soon after the initial retardation. At a test temperature of 650 °C, crack growth retardation, followed immediate acceleration, is also seen upon transferring from fatigue loading to dwell-fatigue loading. However, the rate of crack growth retardation reduces with an increase of ΔK and this period of retardation then led to stable (accelerating) crack growth for ΔK values larger than 32 MPa$\sqrt{m}$ (see for example the second dwell period in 709–3, Fig. 3). Crack growth resistance curves measured from these two tests are relatively consistent apart from in the high ΔK range (> 40 MPa$\sqrt{m}$) where some variations are seen. At the test temperature of 750 °C hardly any crack growth retardation is observed, immediate acceleration and steady state crack growth are seen during all dwell-fatigue segments and following transfer from fatigue cycling (Fig. 4). Despite differences in detail, for crack growth behaviour at different temperatures; it is generally observed that crack growth rates in any stable crack growth region increase with an increase of test temperature. For example, for tests at temperatures of 550 and 650 °C, under a ΔK of 35 MPa$\sqrt{m}$, an increase of less than three times over baseline fatigue crack growth rates is found, whereas increases of ~ 13 times over baseline rates at the test temperature of 750 °C is observed. Estimations of Paris constants based on the crack growth resistance curves after stable crack growth has established, are provided in Table 3.

Note that for the single test conducted in vacuum at a temperature of 650 °C, similar behaviour to that of tests conducted in air has been observed for $\Delta K < 40$ MPa$\sqrt{m}$. The crack growth rates found with $\Delta K >$ 40 MPa$\sqrt{m}$ again show some variation. Another test was conducted on a conventional Type 316H stainless steel (a high carbon variant of 316 austenitic stainless steel), at a temperature of 650 °C in air, under exactly similar testing conditions. Compared to Alloy 709 crack growth rates measured for 316H are much faster than those measured at the same temperature (650 °C) and are almost equivalent to those measured for Alloy 709 at the much higher testing temperature of 750 °C, see Fig. 5.

It is worth mentioning that crack growth under 0.25 Hz cycling obtained after dwell-fatigue block loading is also different to that obtained using baseline loading (0.25 Hz) alone. Upon transfer from dwell-fatigue loading to cyclic (0.25 Hz) loading, reduced crack growth rates are measured consistently. After some crack extension, crack growth rates gradually return to those measured from baseline fatigue loading alone. It is plausible that under this fatigue cycling, cracks re-sharpen gradually and any influence of the prior dwell-fatigue loading history is then eventually removed. The depth of the region being affected varies according to the conditions at transfer but is typically around 1 mm.

3.2. Fractography and metallography

Optical images of typical fracture surfaces can be seen in Fig. 6. Most dwell-fatigue crack growth segments can be easily distinguished on the fracture surfaces as bands except for the first dwell-fatigue period in 709–3 (tested at 650 °C in air). Detailed SEM fractographic observations were conducted with a focus on the dwell-fatigue crack growth regions. Note that a fractographic study of fatigue crack growth alone is reported elsewhere [18].

3.2.1. Tests carried out at a temperature of 550 °C

Compared to predominantly transgranular striated crack growth under fatigue loading (0.25 Hz, $R = 0.1$), various fracture surface morphologies are observed under 1 h dwell-fatigue loading in Alloy 709, depending on the value of ΔK. Based on observations from two tests, the fracture surface morphology remains largely the same as for baseline cycling when ΔK is less than 27 MPa$\sqrt{m}$ (within the first dwell-fatigue cycles of both tests). An example is shown in Fig. 7 (709–1, $\Delta K = 20$ MPa$\sqrt{m}$). It can be seen in Fig. 7 that the first baseline fatigue region is covered with a thick oxide scale which produces clear contrast to the

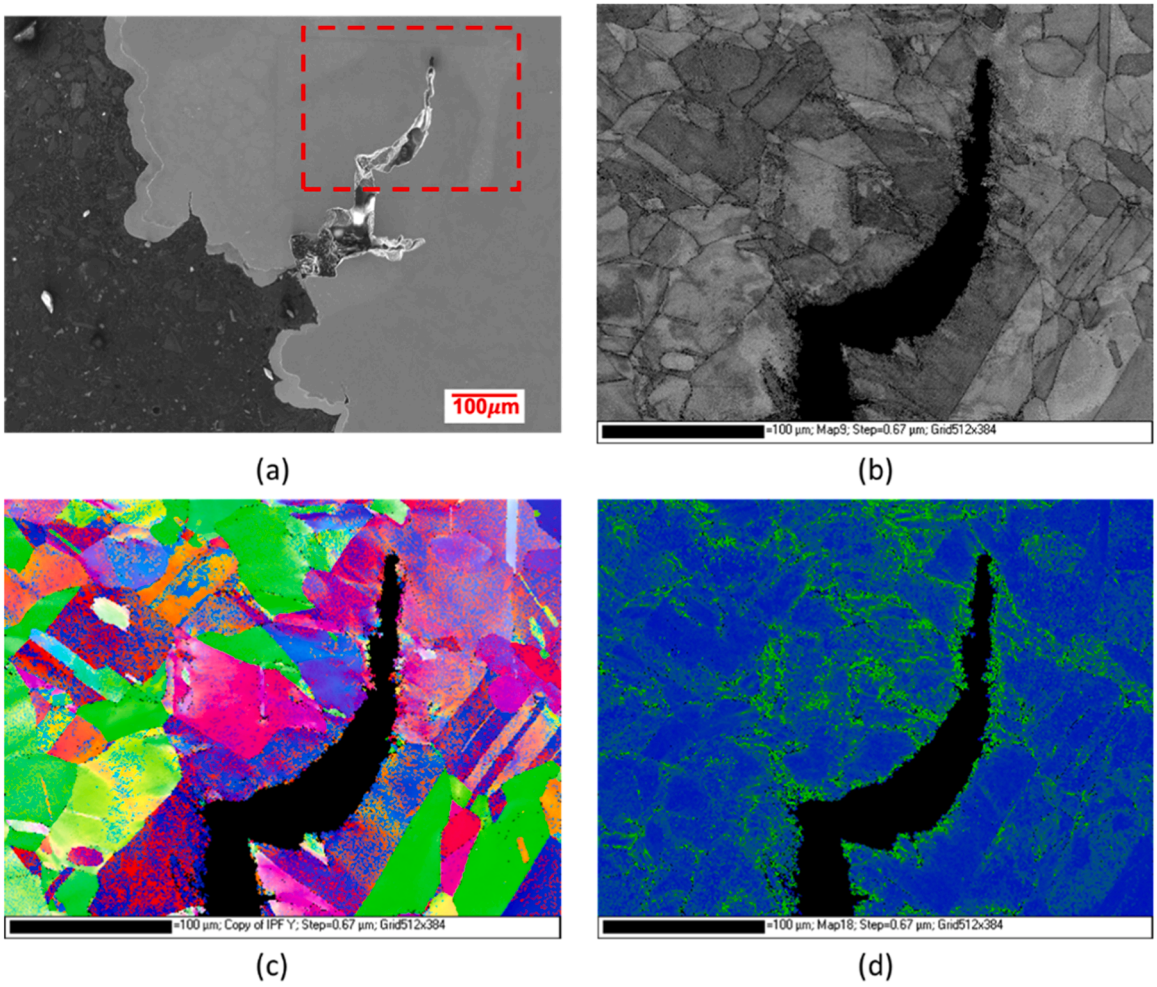

Fig. 10. EBSD results conducted on the metallographic section of the fractured 709–2 (550 °C) at a location of ΔK~36 MPa$\sqrt{m}$ within the second 1 h dwell fatigue crack growth region confirming a transgranular secondary crack: (a) secondary electron image; (b) EBSD band contrast map; (c) crystal orientation map; and (d) local misorientation map marked by rainbow colour, ranging from 0 (blue) to 6° (bright green).

first dwell-fatigue crack growth region. The extent of the first dwell-fatigue region can be recognised with a mark which appears continuous and relatively straight. Clear fatigue striations can be seen throughout, and a comparison of fatigue striations found at the beginning and end of the dwell-fatigue crack growth region is shown in Fig. 7b and c. These striation spacings are ~0.8 and ~0.3 μm at the beginning, and end of the region respectively. This is in general agreement with average crack growth rates predicted by d.c.p.d., and notably with the decrease in crack growth rates measured over this period of dwell-fatigue loading.

In the second dwell-fatigue crack growth region (ΔK values > 32 MPa$\sqrt{m}$), the fracture surface morphology is now completely different and appears "intergranular" at low magnifications, as shown in Fig. 8. Despite this "intergranular" appearance, crack growth rates demonstrate continuous deceleration (after an initial acceleration), even for test-piece 709–2 which was allowed to grow for a longer distance – double that of the second dwell-fatigue region of 709–1. Therefore, stable and continuous increase in crack growth rate with ΔK increases has not been observed in both tests. From observations under higher magnifications, it becomes clear that intergranular areas are discontinuous and are then linked by fatigue striations – presumed to be growing transgranularly. Close-ups of fatigue striations produced at the beginning of, and then in the middle of, the dwell-fatigue loading are shown in Fig. 8b and c respectively. At the beginning of dwell-fatigue loading, striations appear almost continuous and parallel to a stretch zone which separates the baseline fatigue crack growth region and this dwell-fatigue crack growth region. The striation spacing just inside the dwell-fatigue region appears larger than that in the baseline region just prior to the dwell-fatigue crack growth region. Further ahead of the stretch zone, an interesting distribution of striated regions has been observed as shown in Fig. 8c. Here they appear to have other orientations with respect to the general crack growth direction. The striations coexist with multiple isolated intergranular islands. It is suspected that isolated intergranular cracks form ahead of the continuous crack front, and eventually link with the advancing of this continuous crack front. Another piece of evidence which supports such an interpretation of this crack growth mechanism is the observation of intergranular islands in the baseline fatigue region ahead of the second dwell-fatigue crack growth region, as shown in Fig. 8d. The intergranular islands are revealed only by subsequent baseline fatigue crack growth. Some coarse striations were also observed adjacent to the intergranular islands. This area is completely surrounded by continuous fine striations with their spacing indicating slower crack growth rate than the baseline fatigue rates. Clearly the intergranular islands must have formed in the previous dwell-fatigue loading.

With further increase of ΔK, third and fourth dwell-fatigue loading produces similar fracture morphology to that seen during the second dwell-fatigue growth region, but obvious grain boundary cavitation (Fig. 9c) and matrix microvoid coalescence around large inclusions (arrowed in Fig. 9b) can now be seen. Continuous fatigue striations next to a stretch zone are still present. In addition to these observations, the

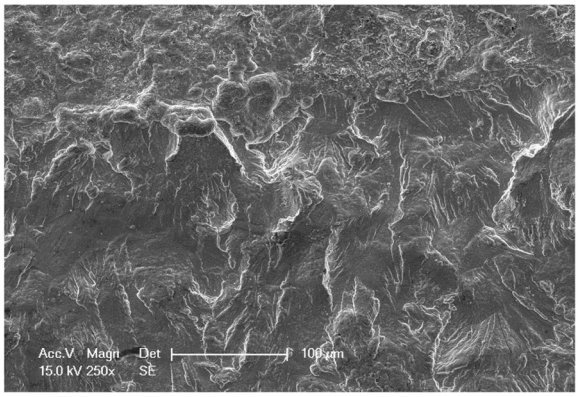

(a)

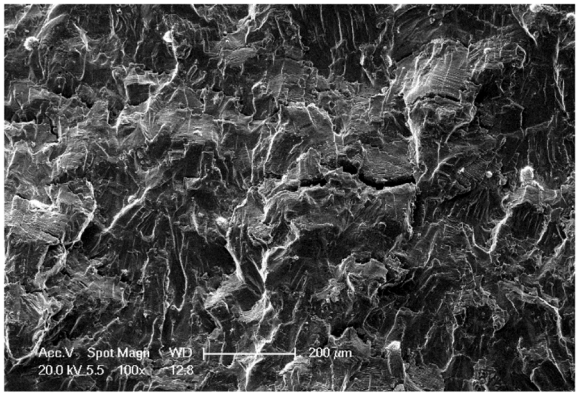

(b)

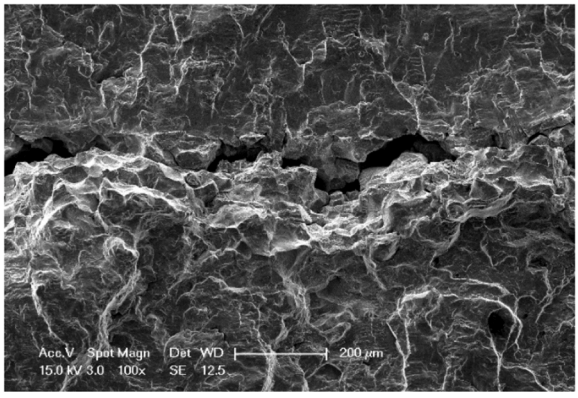

(c)

Fig. 11. SEM fractographs taken from the first dwell-fatigue region of the tests conducted at 650 °C: (a) 709–3, ΔK = 17.8–18.3 MPa$\sqrt{m}$; (b) 709–4, ΔK = 26.9–27.6 MPa$\sqrt{m}$; and (c) 709–5, ΔK = 30.5–31.9 MPa$\sqrt{m}$.

grains retain their sharp edges and equiaxed shape, suggesting a relatively small amount of matrix deformation at this temperature even under severe loading, ΔK is now > 41.7 MPa$\sqrt{m}$, and the nominal stress at the crack tip is estimated at 645 MPa.

To investigate the characteristics of deformation on the crack path at 550 °C, EBSD examination was carried out on the metallographic section of 709–2 at a location of ΔK~36 MPa$\sqrt{m}$ within the second 1 h dwell-fatigue region. Results are shown in Fig. 10, and as can be confirmed from the band contrast map (Fig. 10b) and γ phase orientation map (Fig. 10c), this local part of the crack is transgranular. The surrounding grains appear to be equiaxed with clear straight edges and sharp grain boundary triple points. On the associated misorientation map (Fig. 10d), higher misorientation angles (represented by the green colour) define grain boundaries and are found along the crack path, indicating localisation and concentration of strain.

3.2.2. Tests carried out at a temperature of 650 °C

Similar to tests carried out at 550 °C, fully striated crack growth (transgranular) was also observed in tests at 650 °C under lower ΔK values up to 27.6 MPa$\sqrt{m}$. This is within the first dwell-fatigue region for the two air tests (709–3 and 709–4). With the slight increase of ΔK value to 30.5 MPa$\sqrt{m}$, crack growth became intergranular, for example in the first dwell-fatigue region of 709–5 (tested in vacuum). A comparison of the fracture surface morphology within the first dwell-fatigue region of these three tests is shown in Fig. 11.

In the second dwell-fatigue region a complete transition to intergranular crack growth occurred in both air tests with ΔK values now higher than 31.8 MPa$\sqrt{m}$, see Fig. 12 for fractographs taken from 709 to 3. In addition to the fully intergranular fracture surface, deep secondary cracks can also be seen between adjacent grains. Towards the end of this second dwell-fatigue region of 709–3, for ΔK values leading to 39.7 MPa$\sqrt{m}$, the grain edges become slightly smoother and less distinctive. Due to a severe oxidation, formation of microvoids on grain boundaries are not clearly observed at the beginning of the region (Fig. 12b) but become apparent towards the end of the region (Fig. 12c). This could partially be due to the reduced degree of oxidation (the total time spent growing the entire region is 31 days), and partially due to their size. For 709–5 which was tested in vacuum and for a much shorter period, examination of the first dwell-fatigue region (ΔK ranging from 30.5 to 31.9 MPa$\sqrt{m}$) is shown in Fig. 13b. Now grain boundary cavitation can be confirmed on the fracture surface, although they can be very indistinctive and shallow in places.

In order to further understand this fully intergranular fracture mechanism, EBSD mapping was conducted on the metallographic section of test-piece 709–4 at a location of a ΔK value of 36 MPa$\sqrt{m}$ inside the second dwell-fatigue region. Results are shown in Fig. 14. The intergranular crack path can be confirmed. In addition, localised formation of subgrains and grain boundary cavitation can also be seen. From the misorientation map (Fig. 14d), it is clear that deformation still occurs local to grain boundary areas. There is also some matrix deformation within grains close to the crack path.

With a further increase of ΔK to above 45.0 MPa$\sqrt{m}$ and in the third dwell-fatigue region of 709–3 and 709–4. The overall fracture surface appears generally flat with observation of microvoids. The fractographs of 709–4 are shown in Fig. 15. This region is also accompanied with local narrowing of sample thickness (necking), see Fig. 6. At this stage the fracture surface has lost any appearance of grain boundaries, as shown in Fig. 15. Although intergranular cavitation damage is developing simultaneously, the fracture mode is consistent with conventional tensile necking failure and believed to be predominantly transgranular. This failure mode is referred as microvoid coalescence (MVC) in Table 2. Associated EBSD mapping was performed, results are shown in Fig. 16, and they support this argument.

3.2.3. Tests carried out at a temperature of 750 °C

At this highest temperature employed, continuous acceleration (no retardation) in crack growth is observed throughout. The fracture surface of the first dwell-fatigue region (ΔK ~ 21 MPa$\sqrt{m}$) has a similar appearance of the second dwell-fatigue region of 709–3 tested at 650 °C (associated ΔK of 32 to 40 MPa$\sqrt{m}$), as shown in Fig. 17a and b. However, the fracture surface appears smoother and lacks sharp and distinct features of grain edges. This suggests a larger degree of, and perhaps, more homogenous deformation. Although the fracture surface is heavily oxidised and microvoids cannot be seen clearly, the fracture mechanism is expected to result from intergranular cracking. This is supported by the work of Lall et al. [5] who conducted *in-situ* SEM dwell-fatigue crack growth tests in Alloy 709. They observed that 1 min dwell time is sufficient for formation of microvoids on grain boundaries,

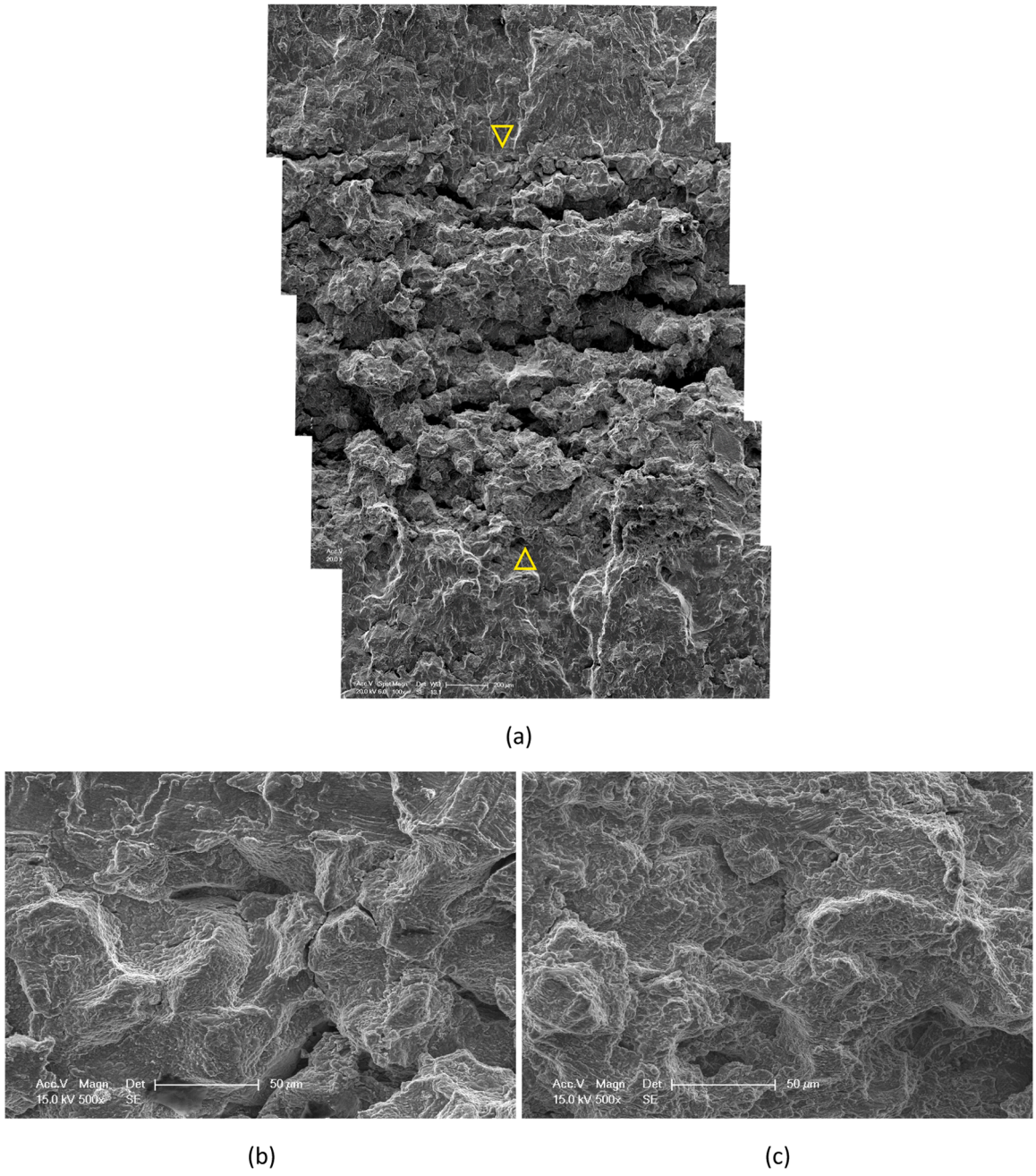

Fig. 12. SEM fractographs taken from the second dwell fatigue crack growth region of the test-piece 709–3 (ΔK ~ 32–40 MPa$\sqrt{m}$) after testing at 650 °C: (a) overview of the region showing predominantly intergranular cracking; (b) and (c) close-up of the beginning and the end of the region; (d) higher magnification of (b). Note that fatigue crack growth direction is from the top to bottom in all cases, also the beginning and end of the dwell fatigue crack growth region are arrowed in (a).

leading to intergranular cracking at 750 °C. In the second dwell-fatigue segment which corresponding to ΔK range of 25.7 to 29.7 MPa$\sqrt{m}$ (Fig. 17c and d), the fracture surface is gradually losing any intergranular appearance. Towards the end of the region, a complete coverage of ductile microvoids is seen. Some microvoids had grown significantly to form a network. Fine microvoids of <5 μm in size can now be seen clearly on the walls of the larger dimples. This failure mode continues to the third dwell-fatigue region with ΔK in the range of 31.9 to 52.7 MPa$\sqrt{m}$, see Fig. 17e and f.

The observed fracture modes are summarised in Table 2 for all dwell-fatigue crack growth regions of individual test-pieces.

4. Discussion

4.1. Mechanism maps

Crack growth rates obtained in Alloy 709 at high temperatures under 1 h dwell-fatigue loading result from competition and/or interaction of two failure processes: cycle-dependant transgranular and striated crack growth, fatigue; and time-dependant damage, creep crack growth. Fig. 18 summaries the failure modes for the three temperatures investigated at three different ΔK values of 20, 35 and 50 MPa$\sqrt{m}$, together with the associated crack growth rates. Addition descriptions of failure modes are provided in Table 5. The crack growth rates obtained under 0.25 Hz are also provided for comparison in Fig. 18. Note that the creep mechanism does not differentiate intergranular cavitation and

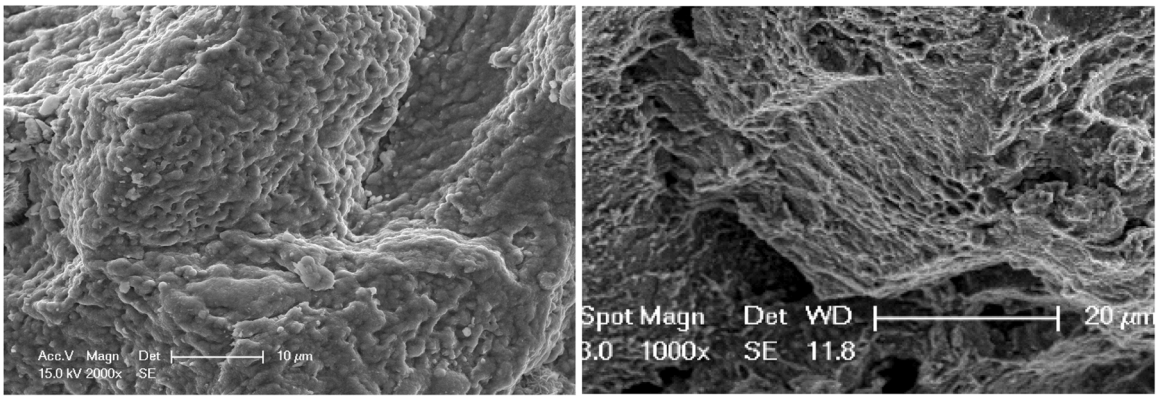

Fig. 13. Comparison of the fracture surface between 709 and 3 (tested in air) and 709–5 (tested in vacuum) at a location of similar ΔK value (~31 MPa$\sqrt{m}$). Note that both tests were conducted at 650 °C.

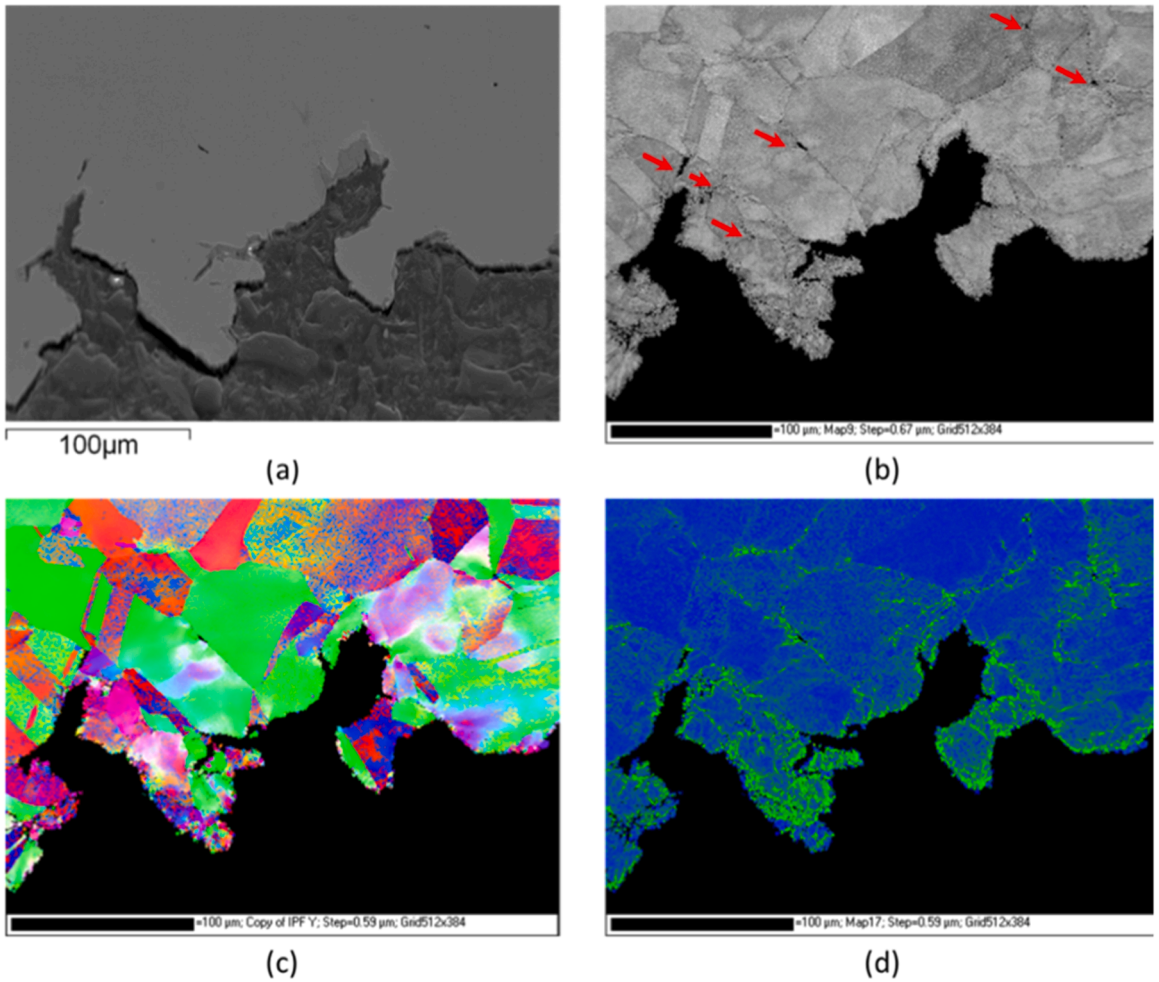

Fig. 14. SEM micrographs of a metallographic section taken at ΔK~36 MPa$\sqrt{m}$ within the second 1 h dwell fatigue crack growth region of 709–4 after testing at 650 °C confirming a intergranular crack profile and limited subgrain formation: (a) secondary electron image; (b) EBSD band contrast map, showing voids formation on grain boundaries (arrowed); (c) crystal orientation map; and (d) local misorientation map marked by rainbow colour, ranging from 0 (blue) to 6° (bright green).

transgranular microvoid coalescence, but details can be found in the previous section. Note also stress intensity factor range (ΔK) is used here as a reference to correlate various failure mechanisms and to make cross comparisons as loading was cyclic. Clearly, it does not represent the "mechanical driving force" for creep crack growth well in the current study. While the appropriate parameter, C*, could not be calculated in the current study without continuous monitoring crack opening displacements, the crack tip nominal stresses resulting from the maximum load are provided in Table 2. In Table 4 some tensile properties of the investigated material are also provided [19–21] for reference.

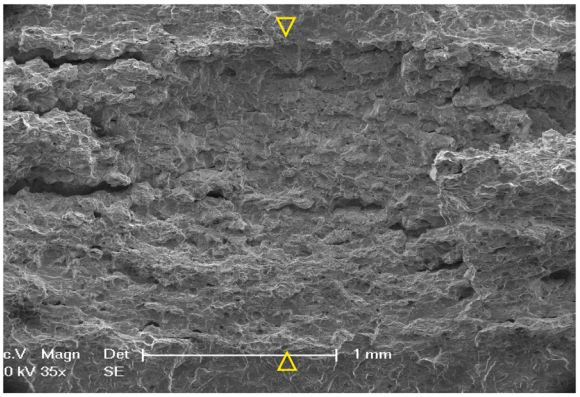

(a)

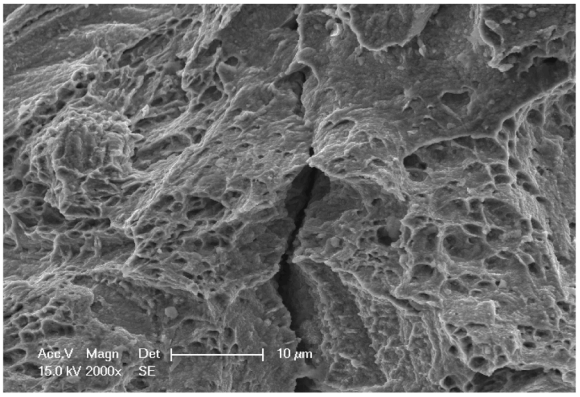

(b)

Fig. 15. SEM fractographs taken from the third dwell fatigue crack growth region of the test-piece 709–4 ($\Delta K \sim 52 - 60$ MPa$\sqrt{m}$) after testing at 650 °C: (a) overview of the region showing a relative smooth morphology; (b) micro-voids becoming directional, indicate rapid shearing. Note that fatigue crack growth direction is from the top to bottom in all cases, also the beginning and end of the dwell fatigue crack growth region are arrowed in (a).

Clear trends of failure mode with temperature and ΔK can be seen in Fig. 18: low ΔK (blue symbols and lines) promotes fatigue; whereas high ΔK (green symbols and line) and high temperature promotes creep crack growth; a transition from fatigue to fully creep damage happens under higher ΔK at lower temperatures, but this did not happen at a temperature of 550 °C. It is only at 550 °C that fatigue-creep interactions are present. In terms of crack growth rates, obvious acceleration over baseline fatigue crack growth rates (dashed lines in Fig. 18), are associated with either high temperatures (> 650 °C) and/or high ΔK values (> 35 MPa$\sqrt{m}$) with fully or partial involvement of creep damage. The individual mechanisms of fatigue, creep and fatigue-creep interaction are considered separately in the following sections.

4.1.1. *Fatigue – negligible creep damage*

As shown in Figs. 7 and 18, a complete transgranular fracture surface morphology can be obtained with a long dwell time of 1 h, i.e. the first dwell-fatigue region at 550 and 650 °C. This highlights the importance of stress level on kinetics of creep damaging process. Taking 650 °C for example the highest crack tip nominal stresses to yield a fully transgranular morphology is 362 MPa (end of the first dwell-fatigue in 709–4, see Table 2). This is larger than the yield stress but smaller than the tensile strength of the alloy at 650 °C (see Table 4). Apparently sufficient creep damage could not develop at or ahead of the growing crack-tip under such combinations of temperature and stress level within the 1 h dwell period, and the failure mechanism remains as a crack tip localised activity – governed by the local stress range and captured using the stress intensity factor range ΔK. Despite a fully transgranular crack growth morphology, crack growth rate features an immediate acceleration followed by sharp retardation. The immediate increase in crack growth rate right after the introduction of tensile dwell can be explained by additional tearing under tensile dwell. This is evident with the observation of a stretch zone, which is significantly larger than the striation spacing just before dwell-fatigue loading. The stretch zone is particularly visible at high driving forces (Fig. 9b). As the crack rapidly gets blunter, presumably with some creep deformation occurring under the tensile dwell, the amount of crack extension per cycle reduces. A comparison of striation spacings between two locations is provided by Fig. 7b and c: at the beginning and at the end of the dwell-fatigue loading region (note the different magnifications in the two micrographs). These striation measurements confirm initial acceleration and later retardation. In addition to such transient crack growth behaviour, it is reasonable to believe that a crack growth rate similar to that measured under 0.25 Hz will also be obtained with 1 h dwell-fatigue loading after it has been stabilised and if the crack path remains transgranular.

4.1.2. *Creep–fatigue interactions*

With an increase of ΔK (nominal stress) and temperature, if more and sufficient creep damage can be accumulated within the 1 h dwell period, then this creep damage could participate in the crack growth process, leading to creep-fatigue interaction. This creep-fatigue interaction occurs particularly at 550 °C under ΔK values higher than 32.9 MPa$\sqrt{m}$. This is evident with an observation of mixed fracture modes of transgranular fatigue striations and intergranular cracking. The nominal (net-section) stress now is around 460 MPa (second dwell-fatigue in 709–1, Table 2) which is still below the tensile strength of the alloy, i.e. 795 MPa (Table 4). Interestingly with a further increase of ΔK to 51.4 MPa$\sqrt{m}$ (corresponding to a nominal (net-section) stress of over 800 MPa) fatigue striations are still present, see Fig. 9b. From Fig. 2 it can be seen that the crack growth rates obtained under this creep-fatigue interaction regime constantly decelerate towards the fatigue crack growth baseline after an initial acceleration. This behaviour is similar to the "fatigue" regime described in Section 4.1.2. Only for ΔK values greater than 41.7 MPa$\sqrt{m}$ (the third dwell-fatigue in 709–1, Table 2), corresponding to a nominal (net-section) stress of greater than 645 MPa, can continuous acceleration in crack growth be obtained. This suggests any creep damaging process at 550 °C is slow, results in relatively low crack growth rates, and as a result complete transition to a creep failure mechanism does not happen. Figs. 8 and 9 demonstrate that the intergranular area can only be linked up by striated transganular growth, which supports this argument. To further interpret the crack growth behaviour at 550 °C, a test was conducted with static loading replacing 1 h dwell-fatigue loading blocks. This static loading was introduced at K values of 31, 39, 45 and 50 MPa$\sqrt{m}$ (corresponding to ΔK values (noting $R = 0.1$) of 29, 36, 41 and 46 MPa$\sqrt{m}$ in the dwell-fatigue tests). For the first three static loading periods (with K values up to 45 MPa$\sqrt{m}$, more than 40 days was spent at each static holding period. However, crack growth tends towards arrest with a total crack extension of less than 0.2 mm. This indicates that fatigue cycling is essential for sustained crack advance at 550 °C. Only at a K value of 50 MPa$\sqrt{m}$ and with a crack tip nominal (net-section) stress higher than the tensile strength, can cracking be continuous. However, a clear difference in crack growth rate between the static loading and dwell-fatigue loading is still seen, as compared in Fig. 19.

Due to limited creep damage at 550 °C, the early stage of creep damage accumulation and the interaction between creep and fatigue mechanisms can be observed clearly. From fracture surfaces of the specimens tested at 550 °C, it can be concluded that isolated creep damages are generated initially, presumably on the sites of high angle grain boundaries or triple points and/or grain boundaries which are relatively normal to the loading axis, within a zone ahead of the sharp fatigue crack tip, as evident from an intergranular island found ~0.4 mm

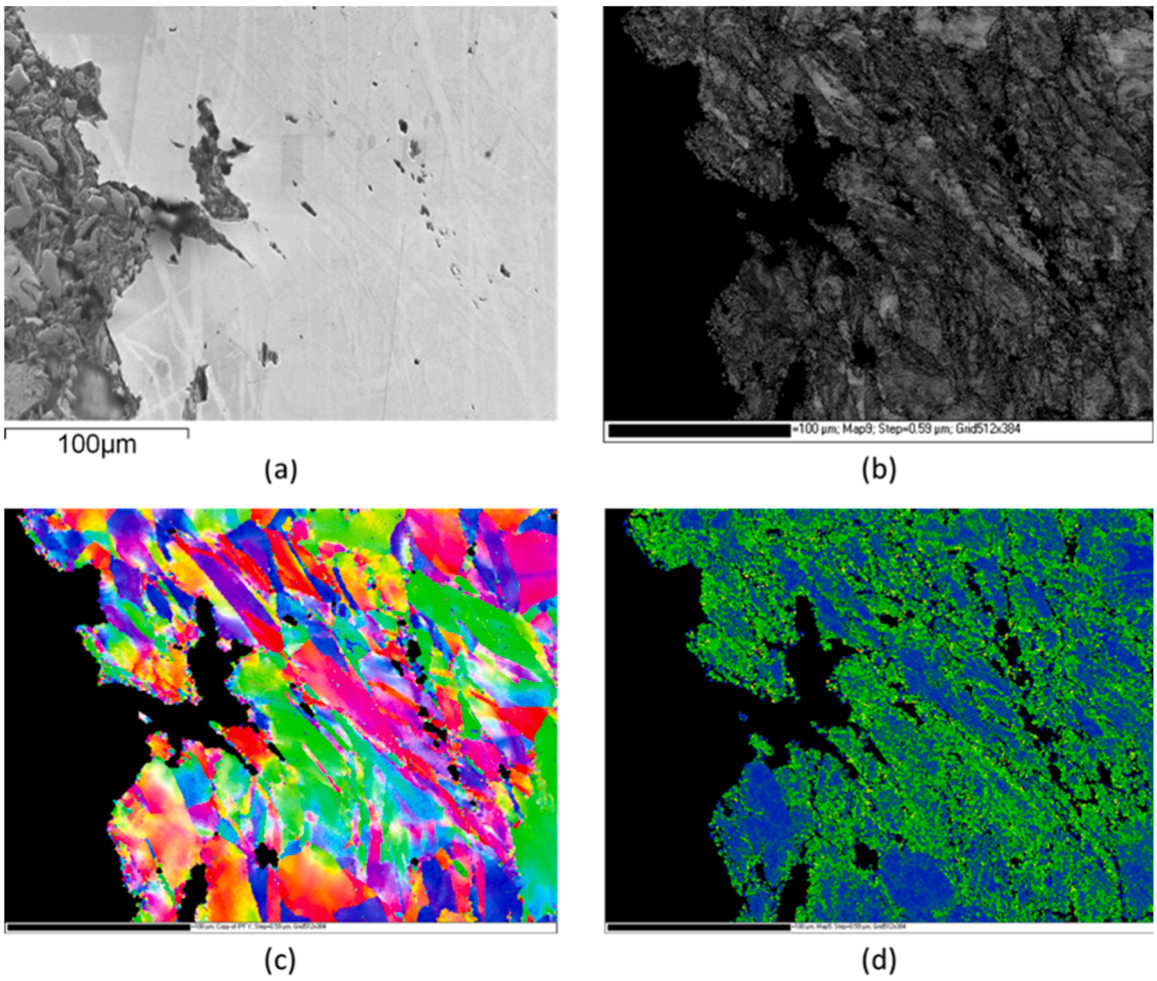

Fig. 16. SEM micrographs of a metallographic section taken at ΔK~50 MPa$\sqrt{m}$ within the third 1 h dwell fatigue crack growth region of 709–2 after testing at 650 °C, showing excessive matrix deformation and subgrain fomation: (a) secondary electron image; (b) EBSD band contrast map; (c) crystal orientation map; and (d) local misorientation map marked by rainbow colour, ranging from 0 (blue) to 6° (bright green).

ahead of the dwell-fatigue region in the fatigue baseline zone. It is reasonable to assume that the fast fatigue cycles after dwell-fatigue loading block can only reveal a small number of intergranular islands that are on the crack path. At 550 °C, the rate to generate creep damage is slow thus only isolated damage can be found on the fracture surface. This has led to the existence of ligaments between the intergranular islands developed. Eventually those uncracked ligaments were linked via transgranular striated growth – fatigue mechanism. It is worth pointing out that fatigue was the dominant mechanism here which drive the crack extension as static load alone could not grow the crack (with K $<$ 45 MPa$\sqrt{m}$), however steady-state crack growth is still difficult to establish except for very high ΔK values.

The excellent resistance against creep crack growth observed in the investigated alloy at 550 °C could have been derived from its deformation characteristics. The deformation mechanisms of Alloy 709 post tensile testing at temperatures of 550, 650 and 750 °C have been investigated by Ding and co-authors [19]. At 550 °C dislocation activity primarily take place in planar form with limited cross-slip. Serrated plastic flow (dynamic strain ageing, DSA) prevails due to impediment of dislocations provided by solute atom of Cr. The material demonstrates the highest degree of strain hardening at 550 °C amongst these three temperatures, leading to the highest tensile strength, i.e., ~800 MPa, achieved just before final fracture. In addition, the material benefits from a range of precipitates including Z-phase (CrNbN type) which predominately forms on dislocations and pins their movement. No obvious necking occurs at this temperature of 550 °C [19]. It is plausible that DSA have contributed to the isolated intergranular cracking at 550 °C during holding period. In fact, a significant reduction in fracture strain has been observed in smooth round bars post stress rupture testing at 550 °C [21]. DSA is often reported to have a detrimental effect on low cycle fatigue life as it introduces heterogenous planar deformation and encourages earlier crack initiation [22–24]. However, no such link is suggested for crack growth resistance. The contribution of DSA on overall crack growth rates here at 550 °C is expected to be minimal. Linkage and accumulation of intergranular fracture seem to rely on creep cavitation, which is extremely slow at 550 °C. As a result, the advance of a continuous crack front can only be achieved by the fatigue mechanism.

4.1.3. Creep crack growth – intergranular cavitation and transgranular microvoid coalescence

As discussed in Section 4.1.1 the failure mode at a temperature of 650 °C and below a ΔK value of 27.6 MPa$\sqrt{m}$ is completely transgranular with fatigue striations. With an increase of ΔK value to 31.8 MPa$\sqrt{m}$ (corresponding to a nominal (net-section) stress of 431 MPa), crack growth has transferred to completely intergranular as mentioned in Section 3.2.2 without showing a phase of creep-fatigue interaction as observed at 550 °C. This fully intergranular crack growth mode appears at a much reduced ΔK of 20.5 MPa$\sqrt{m}$ (corresponding to a nominal (net-section) stress of 232 MPa) with a further increase of temperature to 750 °C. The fact that fully intergranular crack growth is observed on the fracture surface indicates that creep damage induced crack growth has

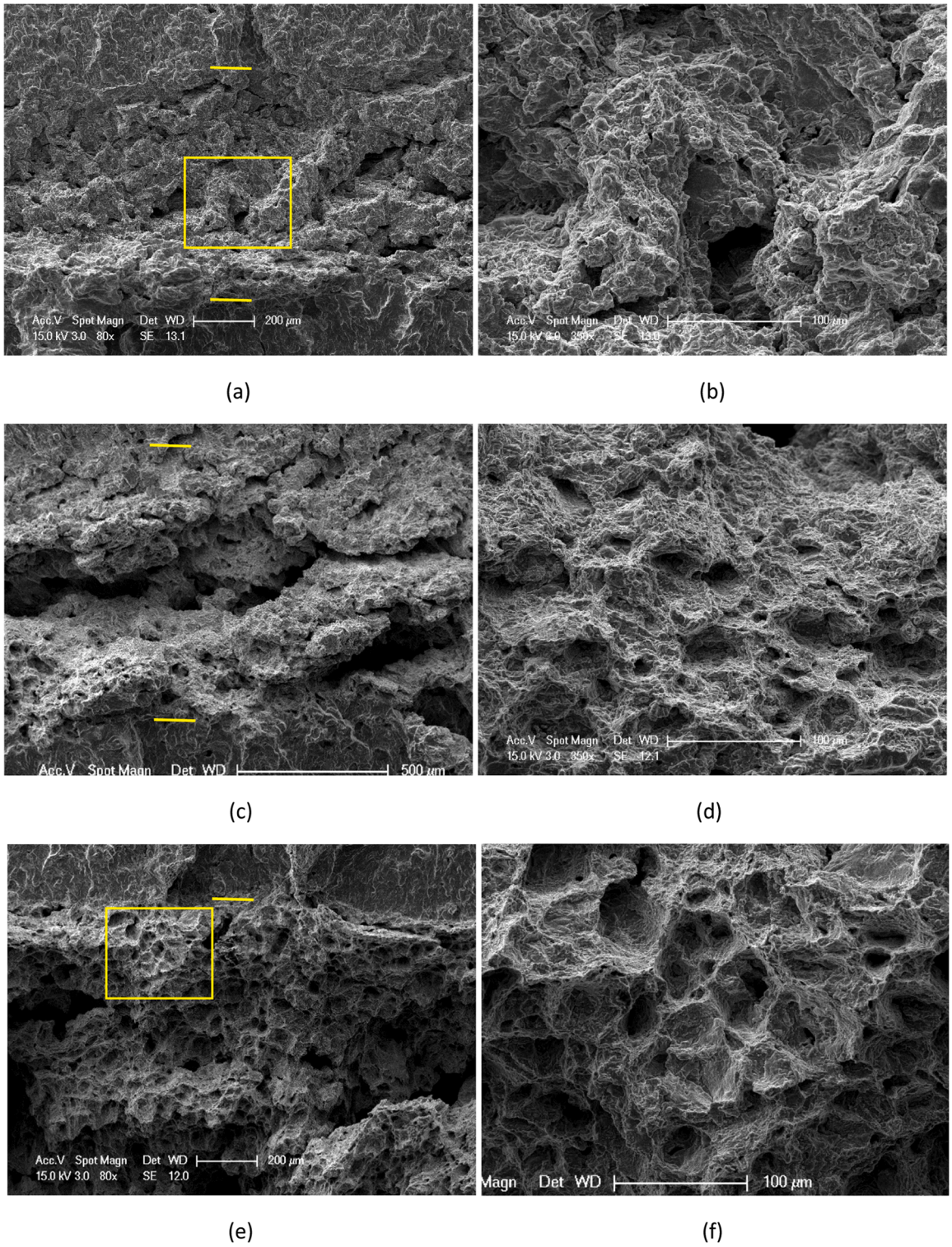

Fig. 17. SEM fractographs of magnifications from the test-piece 709–6 after testing at 750 °C: (a) and (b) the first dwell region (ΔK = 20.5 – 22.2 MPa$\sqrt{m}$); (c) and (d) the second dwell region (ΔK = 25.7 – 29.7 MPa$\sqrt{m}$); (e) and (f) beginning of the third dwell region (ΔK >31.9 $\sqrt{m}$). Note that fatigue crack growth direction is from the top to bottom, also the beginning of the dwell fatigue crack growth region is indicated in all cases.

now overtaken crack growth rate caused by fatigue and become the dominant crack growth mechanism. It seems that temperature has a profound influence on creep crack growth. Only at a temperature higher than 550 °C, can creep damage dominate the crack growth mechanism. When comparing Figs. 3 and 4, contrasting creep crack growth behaviour is seen between 650 and 750 °C with onset of stable creep crack growth, i.e. crack growth rate increases with increase of ΔK. At 650 °C, it is established after a sharp deceleration, whereas at 750 °C the initial deceleration is mild before continuous acceleration. In addition, stable creep crack growth is much slower at 650 °C, with only a moderate (~twice) increase in crack growth rates measured over baseline fatigue. A tenfold increase in crack growth rate is seen at 750 °C. The deceleration phase observed presumably implies that a creep damage zone sustaining stable crack growth needs time to establish, i.e. ~200 h for

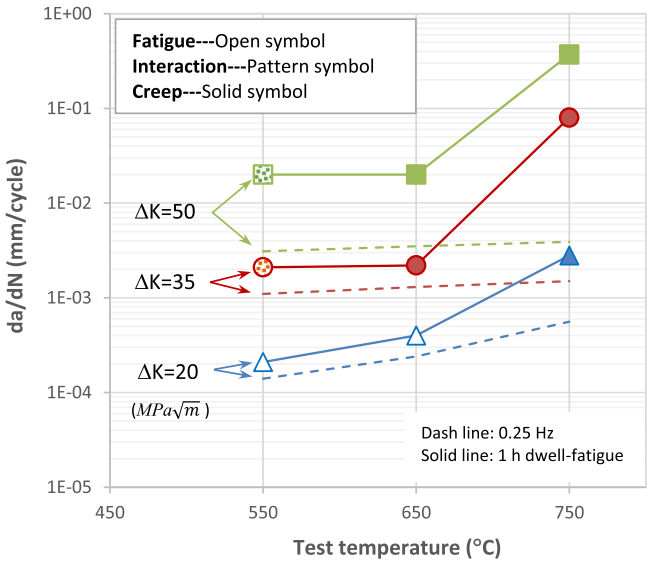

Fig. 18. Overview of failure mechanisms with respect of test temperature and applied ΔK under 1 h dwell-fatigue loading condition in Alloy 709. The associated crack growth rate is also shown and compared to that measured under 0.25 Hz fast fatigue loading. Note that the failure mechanism for all 0.25 Hz condition is fatigue (transgranular with fatigue striations).

Table 4
Yield stress, tensile strength (TS) and fracture stress of Alloy 709 at different temperatures.

T (°C)	0.2% Proof Stress, σ_{YS} MPa	Tensile Strength, TS	Fracture Stress σ_f
550	170	795	1345
650	168	611	741
750	165	378	576

the second dwell-fatigue region of 709–3 and only ~4 h for the third dwell-fatigue region (equivalent ΔK to the second dwell fatigue region of 709–3) at 750 °C. The insignificant deceleration phase seen at 750 °C implies that significant less incubation time is required to establish sustainable creep crack growth.

With further advance of the crack and concomitant increase of ΔK, the nominal (net-section) stresses at and ahead of the crack tip increase, intergranular fracture is then accompanied with various degrees of matrix deformation, as confirmed with an EBSD mapping taken at ~46 MPa$\sqrt{m}$ of ΔK at 650 °C. Finally, the fracture mode turns into near complete microvoid coalescence and undergoes plastic collapse (Figs. 15 and 17). Note that the transition into a complete "ductile fracture" occurred at ΔK values of ~40 and ~27 MPa$\sqrt{m}$ for 709–3 (650 °C) and 709–6 (750 °C) respectively, which roughly correspond to nominal (net-section) stresses at the crack tip reaching the tensile strength of the alloy. It should be noted that at these two temperatures, cross-slip becomes easier, leading to larger and more homogeneous deformation. At 750 °C, dynamic recovery and recrystallisation are believed to occur as has been confirmed even during much shorter periods of testing in a tensile test [19]. This gives rise to a well- developed and uniform microvoid coalescence network at 750 °C. Note that the ductile fracture mode observed in such dwell-fatigue tested samples is consistent to that observed after plane-sided tensile and creep (stress-rupture) testing [19, 21].

Creep deformation and damage is a time-dependant (static) failure process. The mechanism involves formation of microvoids on grain boundaries ahead of crack tip under static stress. These microviods then link up and back to crack front. This fashion of damage development has been confirmed at 550 °C (Section 4.1.2) and is also deduced to be the

Table 5
Summary of fractographic observations under various combination of test temperature and stress (ΔK) conditions. Note that the dwell time is fixed at 1 h.

Temperature (°C)	DK (MPaÖm) 20	35	50
550	Flat transgranular morphology with observation of fatigue striations	Mixture of transgranular fatigue striations and intergranular cracking without visible microvoids on grain boundaries, limited matrix deformation	Mixture of transgranular striations and intergranular cracking with visible microvoids on grain boundaries, limited matrix deformation
650	Flat transgranular morphology with observation of fatigue striations	Completely intergranular cracking. Microvoids on grain boundaries becoming visible. Deformation concentrates around grain boundaries	Fracture may not be completely intergranular. Severe matrix deformation with fine shearing microvoids.
750	Intergranular cracking without visible microvoids. Some matrix deformation.	Complete microvoid coalescence with observation of fine (<5 μm) microvoids and blown-up dimples of various sizes. Severe and homogeneous matrix deformation	Complete microvoid coalescence with observation of fine microvoids and blown-up dimples of various sizes. Severe and homogeneous matrix deformation

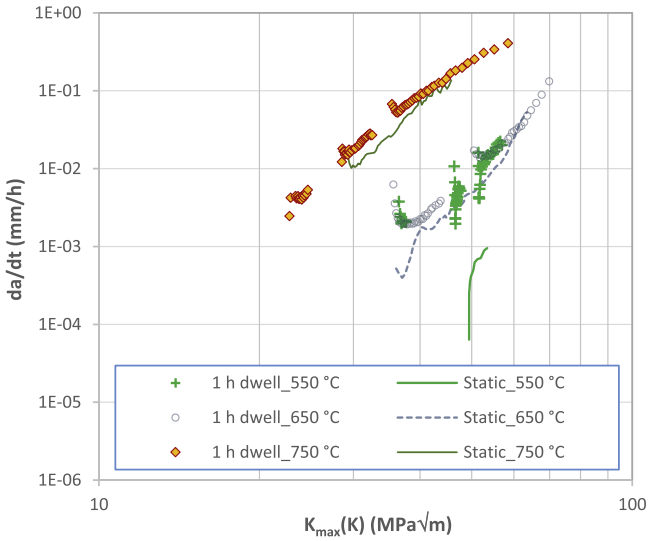

Fig. 19. Comparisons of crack growth rates obtained at 550, 650 and 750 °C under 1 h dwell fatigue loading and the static loading.

case at 650 and 750 °C. As creep damage occurs in a volume of material ahead of crack tip, creep crack growth resistance should therefore be independent of test environment. To confirm this, a test was conducted in vacuum following the same test procedure at a temperature of 650 °C. Fig. 3 presents comparisons of the results from this test (709–5) and two other tests conducted in air. Note that crack growth data obtained under 0.25 Hz alone both in air and in vacuum are also shown in Fig. 3. As can be seen in Fig. 3, there is a subtle but clear difference in crack growth resistance curve between the air and vacuum environments under 0.25 Hz faster cycling and corresponding to striated transgranular fatigue

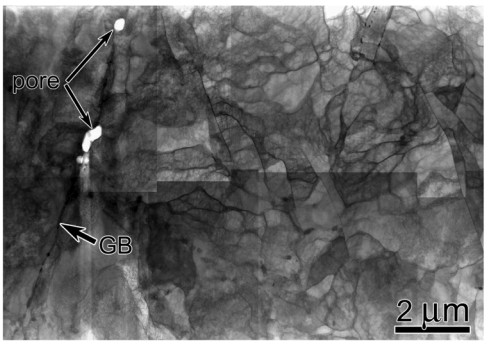

(a)

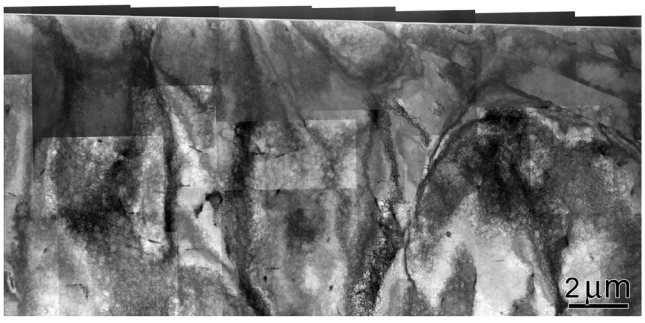

(b)

Fig. 20. Comparison of dislocation substructure between Type 316H and Alloy 709 after testing at 650 °C under 1 h dwell fatigue loading ($\Delta K \sim 35$ MPa$\sqrt{m}$): (a) a montage of bright-field scanning electron transmission electron microscopy (BF-STEM) images showing formation of a larger amount of subgrains and pores on the grain boundary in 316H; and (b) a montage of BF-STEM images showing a high density of dislocations and no evidence of subgrain in Alloy 709.

crack growth. This indicates that an oxidising environment does accelerate crack growth rates under a fatigue mechanism alone. It is understood that the failure process zone for fatigue crack growth in continuous ductile metal is localised at crack tip. This allows access of oxygen and its reaction with the crack tip material which leading to additional damage. A more detailed study is presented elsewhere [18]. However, under 1 h dwell-fatigue loading, the overall crack growth behaviour and growth rates measured in all tests are closely similar for ΔK (K_{max}) values up to 40 MPa$\sqrt{m}$. Although stable (continuous) crack growth has not been reached for the vacuum test and one air test, it would be expected the 709–5 (vacuum test) would have similar crack growth rates to those of 709–3 (air test) should it have been allowed to grow further. This would suggest little influence of air environment and support the earlier argument that creep crack growth is not a crack-tip localised phenomenon. Sadamanda and Shahinian [6] also found that crack growth in Type 304 and 316 austenitic stainless steels at a temperature of 600 °C is independent of environment under dwell-fatigue loading, but slightly faster in air (compared to a vacuum environment) under fatigue loading.

Note that some different crack growth rates can be seen in the last dwell-fatigue region. The mechanism of crack growth in all three tests have seen to have developed into microvoid coalescence- essentially plastic collapse as mentioned in Section 3.2.2.

4.2. Crack growth rates under 1 h dwell-fatigue

4.2.1. Modelling

With an involvement of both fatigue cycling and static hold (at the maximum load), it seems logical to derive the crack growth rate under dwell-fatigue loading as a linear summation of two separate contributions as

$$\frac{da}{dN_{\text{dwell}-\text{fatigue}}} = \frac{da}{dN_{\text{fatigue}}} + \frac{da}{dt_{\text{creep}}} \cdot t_{\text{dwell time}} \quad (2)$$

where $\frac{da}{dN_{\text{fatigue}}}$ and $\frac{da}{dt_{\text{creep}}}$ are the crack growth rates obtained under fatigue and creep (static) conditions, and $t_{\text{dwell time}}$ is the dwell period.

Here we need to bring in crack growth resistance curves under static loading in order to evaluate this concept. In Fig. 19, crack growth resistance curves of creep alone and dwell-fatigue mechanisms are compared. The comparison between fatigue and dwell-fatigue mechanisms have been discussed in previous section and can be found in Figs. 2–4. Note that separate studies on fatigue crack growth alone are presented elsewhere [18] and creep crack growth alone will be presented in another article. Note also that the applied maximum load and test-piece geometry were kept the same for all three types of tests. As some transient crack growth was seen in some cases, only data after establishing stable crack growth before the occurrence of global ductile fracture, are compared.

As discussed previously, dwell-fatigue crack growth at 650 °C ($\Delta K >$ 31.8 or $K_{max} >$35.3 MPa$\sqrt{m}$) and 750 °C is dominated by intergranular creep crack growth. In Fig. 19 crack growth rates obtained under dwell-fatigue and static loading are similar, but slightly slower crack growth rates are seen for the static loading case. This effect seems more significant under low K values and disappear toward high K values where the failure is turning to plastic collapse (stable ductile tearing). Taking $K =$ 30 MPa$\sqrt{m}$ at 750 °C for example, the difference between dwell-fatigue and static loading is $\sim 6.7 \times 10^{-3}$ mm/h. The fatigue crack growth rate of the fatigue mechanism (0.25 Hz) under an equivalent K_{max} ($\Delta K = 27$ MPa$\sqrt{m}$) is $\sim 1.4 \times 10^{-3}$ mm/cycle; if we then choose a K value of 43 MPa$\sqrt{m}$ at 650 °C, the difference between dwell-fatigue and static loading is $\sim 1.5 \times 10^{-3}$ mm/h, whereas the fatigue crack growth rate under fatigue alone under an equivalent K_{max} ($\Delta K = 38.7$ MPa$\sqrt{m}$) is $\sim 1.6 \times 10^{-3}$ mm/cycle. It seems that Eq. (2) roughly works for both these cases.

For the "creep-fatigue" interaction mechanism occurred at 550 °C, creep crack growth alone is not sustained, stable (continuous) crack growth can only be achieved under dwell-fatigue loading, driven by the cyclic transgranular crack growth mechanism. Similar to baseline fatigue crack growth rates would be predicted from Eq. (2) which also is approximately the case, see Figs. 2 and 19.

Although observations are limited here, Eq. (2) can in general give reasonable predictions of crack growth rates under dwell-fatigue loading for a dwell time of 1 h based on crack growth data from separate fatigue crack growth and creep crack growth curves. Such an approach is attractive as crack growth rates under dwell-fatigue loading with any given dwell times can be predicted.

4.3. Comparisons between Alloy 709 to Type 316H

Alloy 709 represents a class of advanced austenitic stainless steels with improved creep strength. The superior creep properties benefit from precipitation hardening due to a variety of stable fine precipices formed during ageing [25]. It is of interest to compare the dwell-fatigue crack growth resistance of Alloy 709 with a conventional solid solution hardened austenitic stainless steels. Here Type 316H, a high carbon version of 316 austenitic stainless steel for elevated temperature applications was selected for such comparison. Fig. 5 compares the results from this test to the results obtained in Alloy 709 at two temperatures of 650 and 750 °C. Multiple tests in 316H have been done following the same procedure and loading parameters as for Alloy 709, but only one representative crack growth resistance curve is shown in Fig. 5. The superior crack growth resistance of Alloy 709 is apparent. Crack growth rates measured in 316H under 1 h dwell-fatigue loading at 650 °C are about 10 times faster compared to those measured in Alloy 709 at the same temperature and are only similar to those of Alloy 709 measured at

a temperature that is 100 °C higher. Although the comparison is only made at 650 °C in order to reduce the testing time, this temperature is higher than the application temperatures of both alloys, it would be expected that advantages of Alloy 709 would persist at lower temperatures.

The mechanism of the superior resistance to dwell-fatigue crack growth of Alloy 709 over 316H is likely to be attributed to strengthening derived from the dispersion of fine precipitates formed after thermal mechanical processing, primarily Nb(CN), and during further thermal exposure, e.g., $M_{23}C_6$, θ ($(Cr,Mo)_3(Ni,Fe)_2SiN$), and Z phases. Amongst them the Z-phases forms on dislocations and effectively pins mobile dislocations [19]. A post-mortem TEM study of the 316H test-piece demonstrates extensive formation of subgrains and microvoids within the second dwell period, see Fig. 20a, indicating that dynamic recovery and recrystallization had already occurred during testing at 650 °C. In contrast, a TEM sample taken from Alloy 709, also within the second dwell-fatigue region after testing at 650 °C, demonstrates primarily a high density of dislocations with only limited subgrains formed along regions close to the crack path (Fig. 20b). This observation suggests a lesser degree of subgrain and dynamic recovery in Alloy 709 at 650 °C, leading to better resistance against creep damage.

5. Conclusions

In this paper, creep-fatigue crack growth behaviour of an advanced austenitic stainless steel Alloy 709 has been investigated at temperatures of 550, 650 and 750 °C using a 1 h maximum load dwell-fatigue waveform ($R = 0.1$). A conventional austenitic stainless steel, Type 316H, was also examined for comparison at 650 °C.

1 Under 1 h dwell-fatigue loading, different crack growth behaviour and failure mechanisms have been observed, resulting from competition and interaction of fatigue and creep failure processes. A mechanism map is provided for the given test-piece geometry and loading conditions
2 It is confirmed that creep crack growth rate increases with an increase of temperature and mechanical driving forces, represented by $\Delta K/K_{max}$ in this study. There is a critical $\Delta K/K_{max}$ value below which creep damage is not competitive and a fully transgranular mechanism will be obtained. This critical ΔK value seems to reduce with an increase of temperature, and is confirmed to be > 26.8 MPa$\sqrt{m}$ at 550 °C and < 20.5 MPa$\sqrt{m}$ at 750 °C. The highest ΔK for observation of a fully fatigue crack growth mechanism at 650 °C is 27.6 MPa$\sqrt{m}$.
3 At 650 and 750 °C crack extension under 1 h dwell-fatigue loading can result solely from a creep mechanism, giving a fully intergranular fracture surface morphology. Contributions from fatigue cycling in such cases are minimal.
4 A fully ductile microvoid coalescence fracture mode is observed prior to final failure at 650 and 750 °C but not at 550 °C. This failure mode occurs at higher ΔK values than those for intergranular creep crack growth, the corresponding K_{max} values are 44 and 30 MPa$\sqrt{m}$ at 650 and 750 °C respectively.
5 Excellent dwell-fatigue crack growth resistance has been observed at 550 °C. Except for very high mechanical driving forces ($\Delta K > 40$ MPa$\sqrt{m}$), stable acceleration in crack growth rate has never been observed under the 1 h dwell-fatigue loading. This is attributed to the excellent creep resistance of the 709 alloy at this temperature. Only isolated and limited creep damage is observed on the fracture surface. Fatigue-creep interactions can be seen only at this temperature.
6 A significant improvement in creep crack growth resistance is achieved with Alloy 709 compared to that of Type 316H austenitic stainless steel when tested at 650 °C.

Author declaration

We wish to confirm that there are no known conflicts of interest associated with this publication and there has been no significant financial support for this work that could have influenced its outcome.

We confirm that the manuscript has been read and approved by all named authors and that there are no other persons who satisfied the criteria for authorship but are not listed. We further confirm that the order of authors listed in the manuscript has been approved by all of us.

We confirm that we have given due consideration to the protection of intellectual property associated with this work and that there are no impediments to publication, including the timing of publication, with respect to intellectual property. In so doing we confirm that we have followed the regulations of our institutions concerning intellectual property.

We understand that the Corresponding Author declared on the title page of the manuscript is the sole contact for the Editorial process (including Editorial Manager and direct communications with the office). She is responsible for communicating with the other authors about progress, submissions of revisions and final approval of proofs. We confirm that we have provided a current, correct email address which is accessible by the Corresponding Author.

Declaration of Competing Interest

The authors declare that they have no known competing financial interests or personal relationships that could have appeared to influence the work reported in this paper.

Acknowledgements

This work was supported by the US Department of Energy (DOE) Nuclear Energy University Program (NEUP) award 2015–1877/DE-NE0008451, and the UK Engineering and Physical Science Research Council award EP/N016351/1.

References

[1] R.A. Ainsworth, R5 procedures for assessing structural integrity of components under creep and creep–fatigue conditions, Int. Mater. Rev. 51 (2006) 107–126.
[2] P. Rodriguez, K. Bhanu Sankara Rao, Nucleation and growth of cracks and cavities under creep-fatigue interaction, Prog. Mater. Sci. 37 (1993) 403–480.
[3] A. Saxena, Creep and creep-fatigue crack growth, Int. J. Fract. 191 (2015) 31–51.
[4] H.Y. Li, J.F. Sun, M.C. Hardy, H.E. Evans, S.J. Williams, T.J.A. Doel, P. Bowen, Effects of microstructure on high temperature dwell fatigue crack growth in a coarse grain PM nickel based superalloy, Acta Mater. 90 (2015) 355–369.
[5] A. Lall, S. Sarkar, R. Ding, P. Bowen, A. Rabiei, Performance of Alloy709 under creep-fatigue at various dwell times, Mater. Sci. Eng. A 761 (2019), 138028.
[6] K. Sadananda, P. Shahinian, Effect of environment on crack growth behavior in austenitic stainless steels under creep and fatigue conditions, Metall. Trans. A 11 (1980) 267–276.
[7] C.S. Chang, PhD thesis, School of Metallurgy and Materials, University of Birmingham (UK, 2000.
[8] L.A. James, Hold-time effects on the elevated temperature fatigue-crack propagation of Type 304 stainless steel, Nucl. Technol. 16 (1972) 521–530.
[9] S. Majumdar, P.S. Maiya, Creep-fatigue interactions in an austenitic stainless steel, Can. Metall. Q. 18 (1979) 57–64.
[10] P. Shahinian, Creep-fatigue crack propagation in austenitic stainless steel, J. Press. Vessel Technol. 98 (1976) 166–172.
[11] X.L. Yan, X.C. Zhang, S.T. Tu, S.L. Mannan, F.Z. Xuan, Y.C. Lin, Review of creep–fatigue endurance and life prediction of 316 stainless steels, Int. J. Press. Vessels Pip. 126-127 (2015) 17–28.
[12] N. Gao, M.W. Brown, K.J. Miller, Crack growth morphology and microstructural changes in 316 stainless steel under creep-fatigue cycling, Fatigue Fract. Eng. Mater. Struct. 18 (1995) 1407–1422.
[13] D.W. Kim, J.H. Chang, W.S. Ryu, Evaluation of the creep–fatigue damage mechanism of Type 316L and Type 316LN stainless steel, Int. J. Press. Vessels Pip. 85 (2008) 378–384.
[14] M. Sauzay, M. Mottot, L. Allais, M. Noblecourt, I. Monnet, J. Périnet, Creep-fatigue behaviour of an AISI stainless steel at 550°C, Nucl. Eng. Des. 232 (2004) 219–236.
[15] R. Piques, P. Bensussan, A. Pineau, Crack initiation and growth under creep and fatigue loading of an austenitic stainless steel, Nucl. Eng. Des. 116 (1989) 293–306.
[16] N. Shaber, R. Stephens, J. Ramirez, G.P. Potirniche, M. Taylor, Fatigue and creep-fatigue crack growth in alloy 709 at elevated temperatures, Mater. High Temp. 36 (2019) 562–574.
[17] ASTM Standard E2760-19e1. Standard testing method for creep-fatigue crack growth testing, ASTM International, West Conshohocken PA, 2020.

[18] S. Yu, J. Yan, H.Y. Li, R. Ding, A. Lall, A. Rabiei, P. Bowen, Fatigue crack growth resistance of the austenitic stainless steel Alloy 709 at elevated temperatures, J. Mater. Res. Technol. 9 (2020) 12955–12969.
[19] R. Ding, J. Yan, H.Y. Li, S. Yu, A. Rabiei, P. Bowen, Deformation microstructure and tensile properties of Alloy 709 at different temperatures, Mater. Des. 176 (2019), 107843.
[20] S. Upadhayay, H.Y. Li, P. Bowen, A. Rabiei, A study on tensile properties of Alloy 709 at various temperatures, Mater. Sci. Eng., A 733 (2018) 338–349.
[21] J. Yan, PhD thesis, School of Metallurgy and Materials, Birmingham University (UK, 2021.
[22] V.S. Srinivasan, R. Sandhya, M. Valsan, K. Bhanu Sankara Rao, S.L. Mannan, The influence of dynamic strain ageing on stress response and strain-life relationship in low cycle fatigue of 316L(N) stainless steel, Scr. Mater. 37 (1997) 1593–1598.
[23] K. Bhanu Sankara Rao, H. Schiffers, H. Schuster, H. Nickel, Influence of time and temperature dependent processes on strain controlled low cycle fatigue behavior of Alloy 617, Metall. Trans. A 19A (1998) 359–371.
[24] Z.Y. Alsmadi, K.L. Murty, High-temperature effects on creep-fatigue interaction of the Alloy 709 austenitic stainless steel, Int. J. Fatigue 143 (2021), 105987.
[25] R. Ding, J. Yan, H.Y. Li, S. Yu, A. Rabiei, P. Bowen, Microstructural evolution of Alloy 709 during aging, Mater. Charact. 154 (2019) 400–423.